REPORT DOCUMENTATION PAGE

Form Approved OMB NO. 0704-0188

1. REPORT DATE (DD-MM-YYYY)	2. REPORT TYPE	3. DATES COVERED (From - To)
05-06-2015	Final Report	9-May-2011 - 8-May-2015

4. TITLE AND SUBTITLE
Final Report: Sparsity Aware Adaptive Radar Sensor Imaging in Complex Scattering Environments

5a. CONTRACT NUMBER
W911NF-11-1-0160

5b. GRANT NUMBER

5c. PROGRAM ELEMENT NUMBER
206022

6. AUTHORS
Yuanwei Jin

5d. PROJECT NUMBER

5e. TASK NUMBER

5f. WORK UNIT NUMBER

7. PERFORMING ORGANIZATION NAMES AND ADDRESSES
University of Maryland - Eastern Shore
11868 Academic Oval

Princess Anne, MD 21853 -1299

8. PERFORMING ORGANIZATION REPORT NUMBER

9. SPONSORING/MONITORING AGENCY NAME(S) AND ADDRESS (ES)
U.S. Army Research Office
P.O. Box 12211
Research Triangle Park, NC 27709-2211

10. SPONSOR/MONITOR'S ACRONYM(S)
ARO

11. SPONSOR/MONITOR'S REPORT NUMBER(S)
58932-EL-REP.25

12. DISTRIBUTION AVAILIBILITY STATEMENT
Approved for Public Release; Distribution Unlimited

13. SUPPLEMENTARY NOTES
The views, opinions and/or findings contained in this report are those of the author(s) and should not contrued as an official Department of the Army position, policy or decision, unless so designated by other documentation.

14. ABSTRACT
In this reporting period, we develop new radar imaging, estimation, and waveform encoding techniques that exploit prior knowledge of the target and its environment to improve system performance through sensing, learning, and exploitation. Our research accomplishment is three fold. First, we develop a variational Bayesian based framework to address the problem of multi-parameter estimation under compound Gaussian clutter in the context of cognitive radar. Results demonstrate an accelerated convergence of the proposed sequential estimation method with an improved asymptotic Cramer Rao bound compared with the conventional expectation-maximization (EM) method

15. SUBJECT TERMS
Image reconstruction, Sparsity, Cognitive Radar, Bayesian Inference, Waveform Design

16. SECURITY CLASSIFICATION OF:			17. LIMITATION OF ABSTRACT	15. NUMBER OF PAGES	19a. NAME OF RESPONSIBLE PERSON
a. REPORT	b. ABSTRACT	c. THIS PAGE			Yuanwei Jin
UU	UU	UU	UU		19b. TELEPHONE NUMBER 410-621-3410

Report Title

Final Report: Sparsity Aware Adaptive Radar Sensor Imaging in Complex Scattering Environments

ABSTRACT

In this reporting period, we develop new radar imaging, estimation, and waveform encoding techniques that exploit prior knowledge of the target and its environment to improve system performance through sensing, learning, and exploitation. Our research accomplishment is three fold. First, we develop a variational Bayesian based framework to address the problem of multi-parameter estimation under compound Gaussian clutter in the context of cognitive radar. Results demonstrate an accelerated convergence of the proposed sequential estimation method with an improved asymptotic Cramer Rao bound compared with the conventional expectation-maximization (EM) method and the classic Bayesian approach, especially under small sample size. Second, we develop estimation method for range and Doppler using weighted OFDM waveforms for radar targets. We demonstrates that the proposed weighted OFDM modulation scheme results in a lower Cramer-Rao bounds for delay estimation compared with the classic constant-envelope OFDM modulation while meeting the requirement on the peak to average power ratio. Third, we study impact of waveform encoding on nonlinear electromagnetic tomographic imaging algorithms using multiple simultaneous excitation sources. By numerical simulations, we show that the proposed iterative image reconstruction algorithm using coded multiple source excitation achieves faster convergence and better quality images than the conventional single source excitation imaging.

Enter List of papers submitted or published that acknowledge ARO support from the start of the project to the date of this printing. List the papers, including journal references, in the following categories:

(a) Papers published in peer-reviewed journals (N/A for none)

Received	Paper
06/03/2015 20.00	Yuanwei Jin, Anish Turlapaty. Bayesian Sequential Parameter Estimation byCognitive Radar With Multiantenna Arrays, IEEE Transactions on Signal Processing, (02 2015): 974. doi:
06/03/2015 21.00	Min Yu, Deshuang Zhao, Yuanwei Jin, Bing-Zhong Wang. Near-Field Image Restoration for Rotman Lensby Localized Angle-Time Spread Function-BasedFiltering Method, IEEE Transactions on Antennas and Propagation, (05 2015): 2353. doi:
08/04/2014 15.00	Chengdong Dong, Yuanwei Jin, Enyue Lu. Accelerated Nonlinear Multichannel Ultrasonic Tomographic Imaging Using Target Sparseness, IEEE TRANSACTIONS ON Image Processing, (03 2014): 1379. doi:
08/26/2013 11.00	Chengdong Dong, Yuanwei Jin. MIMO Nonlinear Ultrasonic Tomography by Propagation and Backpropagation Method, IEEE TRANSACTIONS ON Image Processing, (03 2013): 1056. doi:
TOTAL:	**4**

Number of Papers published in peer-reviewed journals:

(b) Papers published in non-peer-reviewed journals (N/A for none)

Received Paper

TOTAL:

Number of Papers published in non peer-reviewed journals:

(c) Presentations

Number of Presentations: 0.00

Non Peer-Reviewed Conference Proceeding publications (other than abstracts):

Received Paper

TOTAL:

Number of Non Peer-Reviewed Conference Proceeding publications (other than abstracts):

Peer-Reviewed Conference Proceeding publications (other than abstracts):

Received		Paper
06/03/2015	22.00	Anish Turlapaty, Yuanwei Jin. Multi-parameter estimation for cognitive radar in compound Gaussian clutter, IEEE International Conference on Acoustics, Speech, and Signal Processing (ICASSP). 19-APR-15, . : ,
08/02/2012	1.00	Yuanwei Jin. Cognitive Multi-Antenna Radar Detection Using Bayesian Inference, IEEE Sensor Array and Multi-Channel Signal Processing Workshop. 10-JUN-12, . : ,
08/02/2012	5.00	Chengdong Dong, Yuanwei Jin, Enyue Lu. Time Domain Electromagnetic Tomography Using Propagation and Backpropagation Method, IEEE International Conference on Image Processing. 01-OCT-12, . : ,
08/02/2012	2.00	Chengdong Dong, Yuanwei Jin, Enyue Lu. Sparsity Aware Nonlinear Multichannel Ultrasonic Tomographic Imaging, IEEE Sensor Array and Multi-Channel Signal Processing Workshop. 17-JUN-12, . : ,
08/04/2014	16.00	Agustin Rivera-Longoria , Mark Idleman, Yuanwei Jin, Pedro D. Bello, Enyue Lu. Graphics Processing Units Accelerated MIMO TomographicImage Reconstruction Using Target Sparseness, SPIE Sensing Technology + Applications conference. 07-MAY-14, . : ,
08/04/2014	17.00	Anish Turlapaty, Yuanwei Jin. A Joint Design of Transmit Waveforms for Radar and Communications Systems in Coexistence, IEEE Radar Conference. 21-MAY-14, . : ,
08/04/2014	18.00	Yuanwei Jin, Yang Xu, Anish Turlapaty. Range and Velocity Estimation of Radar Targets by Weighted OFDM Modulation, IEEE Radar Conference. 20-MAY-14, . : ,
08/26/2013	8.00	Anish Turlapaty , Yuanwei Jin. Parameter estimation and waveform design for cognitive radar by minimal free-energy principle, IEEE International Conferences on Acoustics, Speech and Signal Processing (ICASSP 2013). 28-MAY-13, . : ,
08/26/2013	9.00	Nicolo Testi, Yang Xu , Yuanwei Jin. Successive-MFCW modulation for ultra-fast narrowband radar, IEEE International Conferences on Acoustics, Speech and Signal Processing. 28-MAY-13, . : ,
08/26/2013	10.00	Pedro D. Bello, Yuanwei Jin , Enyue Lu. GPU accelerated MIMO ultrasonic imaging using propagation and backpropagation, IEEE China Summit and Signal and Information Processing Conference. 08-JUL-13, . : ,

TOTAL: **10**

Number of Peer-Reviewed Conference Proceeding publications (other than abstracts):

(d) Manuscripts

Received		Paper
06/03/2015	23.00	Yuanwei Jin, Chengdon Dong, Enyue Lu. Waveform Encoding for Nonlinear Electromagnetic Tomographic Imaging, IEEE Global Conference on Signal and Information Processing (05 2015)
06/03/2015	24.00	Amir Asif, Yuanwei Jin, Foroohar Foroozan. Cramer-Rao Bounds for Time Reversal MIMO Radars with Multipath, IEEE TRANSACTIONS ON AEROSPACE AND ELECTRONIC SYSTEMS (02 2015)
08/02/2012	3.00	Chengdong Dong, Yuanwei Jin, Enyue Lu. Accelerated Nonlinear Multichannel Ultrasonic Tomographic Imaging Using Sparsity Constraints, SIAM Journal on Imaging Science (07 2012)
08/02/2012	4.00	Chengdong Dong, Yuanwei Jin. MIMO Nonlinear Ultrasonic Tomography by Propagation and Backpropagation Method, IEEE Transactions on Image Processing (10 2011)
08/26/2013	12.00	Anish Turlapaty, Yuanwei Jin. A Unified Approach for Parameter Estimation and Waveform Design By Free-Energy Principle, IEEE TRANSACTIONS ON Signal Processing (08 2013)
08/26/2013	13.00	Anish Turlapaty , Yuanwei Jin. Sequential Bayesian Parameter Estimation by Cognitive Multi-Antenna Arrays, IEEE TRANSACTIONS ON Signal Processing (07 2013)
TOTAL:		**6**

Number of Manuscripts:

Books

Received		Book
TOTAL:		

Received	Book Chapter

TOTAL:

Patents Submitted

May 18, 2015 a provisional patent application titled "Weighted OFDM Modulation Technology for Radar Parameter Estimation" was filed to the US Patent and Trademark Office. Provisional patent application no. 62/162962. Authors: Anish Turlapaty, Yuanwei Jin, and Yang Xu

Patents Awarded

Awards

Graduate Students

NAME	PERCENT_SUPPORTED
FTE Equivalent:	
Total Number:	

Names of Post Doctorates

NAME	PERCENT_SUPPORTED
Anish Turlapaty	1.00
FTE Equivalent:	**1.00**
Total Number:	**1**

Names of Faculty Supported

NAME	PERCENT_SUPPORTED	National Academy Member
Yuanwei Jin	0.11	
FTE Equivalent:	**0.11**	
Total Number:	**1**	

Names of Under Graduate students supported

NAME	PERCENT_SUPPORTED
FTE Equivalent:	
Total Number:	

Student Metrics

This section only applies to graduating undergraduates supported by this agreement in this reporting period

The number of undergraduates funded by this agreement who graduated during this period:	0.00
The number of undergraduates funded by this agreement who graduated during this period with a degree in science, mathematics, engineering, or technology fields:.....	0.00
The number of undergraduates funded by your agreement who graduated during this period and will continue to pursue a graduate or Ph.D. degree in science, mathematics, engineering, or technology fields:.....	0.00
Number of graduating undergraduates who achieved a 3.5 GPA to 4.0 (4.0 max scale):.....	0.00
Number of graduating undergraduates funded by a DoD funded Center of Excellence grant for Education, Research and Engineering:.....	0.00
The number of undergraduates funded by your agreement who graduated during this period and intend to work for the Department of Defense	0.00
The number of undergraduates funded by your agreement who graduated during this period and will receive scholarships or fellowships for further studies in science, mathematics, engineering or technology fields:	0.00

Names of Personnel receiving masters degrees

NAME

Total Number:

Names of personnel receiving PHDs

NAME

Total Number:

Names of other research staff

NAME PERCENT_SUPPORTED

FTE Equivalent:

Total Number:

Sub Contractors (DD882)

Inventions (DD882)

Scientific Progress

Radar imaging and parameter estimation can be modeled as an inverse problem: y = R(f) + w, i.e., from noisy measurement vector y to reconstruct or estimate the target parameter vector f, which could be the spatial reflectivity coefficient vector or other target properties. The operator R (linear or nonlinear) depends on many factors such as the waveform transmission strategy, the data collection geometry, the medium property, and the underlying wave propagation models. A fundamental question that this project aims to address is: how to explore novel waveform transmission, modulation, and statistical computing techniques to achieve superior imaging and parameter estimation.

The main accomplishments of the project during this reporting period are (1) the development of multi-parameter estimation methods for cognitive radar under compound Gaussian clutter using variational Bayesian inference; 2) the development of range and Doppler estimation method using weighted OFDM modulation, and 3) the development of novel microwave nonlinear image reconstruction algorithm using waveform encoding schemes. A summary of the accomplishments is provided below. Detailed technical descriptions are provided in the attached publications and manuscripts.

Accomplishment 1: Development of Multi-Parameter Estimation Method for Cognitive Radar Under Compound Gaussian Clutter Using Variational Bayesian Inference

Cognitive radar has been proposed as a fully adaptive radar transmission and reception system [1]. In cognitive radar, both the transmitter and the receiver parameters are estimated and updated by learning from the unknown environment, forming a belief on what is learned, and propagating this belief by Bayesian inference. From the parameter estimation perspective, the Bayesian approach enables inclusion of prior information (knowledge) of radar target and clutter by estimating the posterior density of the unknown parameters. The estimation is optimal in the sense of minimizing the Bayesian mean squared error (MSE). Typically, the full joint probability density function (pdf) of all the parameters of interest including the nuisance parameters is considered. However, in the case of high-dimensional multi-variate integration of Bayesian posterior density, the calculation of the posterior pdf and its marginal can be computationally prohibitive and tractable analytical solutions are often not available. Furthermore, the estimation accuracy is directly related to the number of data samples in the Bayesian estimator. However, in many radar applications, the number of available data samples is limited. These computational challenges and limitations must be addressed to develop next generation cognitive radar.

In this work, we developed a variational Bayesian (VB) based method for parameter estimation. Variational Bayesian aims to minimize free energy [2, 3], which is equivalent to minimizing the Kullback-Liebler divergence between the true posterior density and an approximation density of the parameters to be estimated. As a result of this functional optimization for density estimation, the marginal VB posterior density has an explicit functional structure, thus leading to closed form solutions [4]. In this work, we focus on multiple parameter estimation of target under compound Gaussian clutter in the context of cognitive radar as an extension of our prior work on single parameter estimation [2]. The compound Gaussian clutter model is used in high-resolution and low-grazing-angle radar to characterize random and non-stationary sea clutter. The Bayesian estimator must consider a multi-parameter estimation problem by which the parameters in the compound-Gaussian model, the radar target response, as well as other nuisance parameters are estimated. We compare the performance of the proposed VB method with the expectation-maximization (EM) algorithm. In the EM method, expectations of sufficient statistics are computed with respect to the posterior density of hidden variables and then used to iteratively estimate the unknown parameters by the maximum likelihood principle. We show that our proposed variational algorithms outperform the EM method particularly when estimating parameters that follow non-Gaussian nonlinear models in Bayesian inference. Hence, the proposed variational algorithms provide appealing computational advantages for cognitive radar. The results have been presented at the IEEE Conference on Acoustics, Speech, and Signal Processing in April 2015 (see Ref. [5]). A more detailed discussion of the VB algorithm has been included in a journal version of the paper (see Ref. [6]).

Accomplishment 2: Development of range and Doppler estimation using weighted OFDM modulation for radar targets.

Estimation of range and velocity of targets is an important problem in radar applications. Orthogonal frequency division multiplexing (OFDM) offers robust system performance in rich multipath fading environment [7]. Challenges with range and velocity estimation of radar targets are the need for high range and Doppler resolutions and resolving phase wrapping. A high range resolution requires a high signal bandwidth while a high Doppler resolution requires long pulse repetition intervals. For OFDM signals, the range resolution depends on the sub-carrier spacing. The resolution improves as the spacing increases. However, since the sub-carrier spacing and the pulse repetition interval are inversely related, there exist trade-offs for achieving high resolutions in both range and Doppler. Next, for fast moving targets such as missiles and airplanes, phase wrapping may appear due to the 2 pi modulo folding, i.e., the actual Doppler frequency is likely to be greater than the corresponding sampling frequency. As a result, discrete Fourier transform (DFT) based sinusoidal estimation methods can only extract the remainder after 2 pi modulo folding. The integer multiple of the sampling frequency that is lost due to phase wrapping is known as the folding error. The time delay estimation corresponding to the range is also subject to a similar phase wrapping problem. Furthermore, phase based parameter estimation methods are generally sensitive to phase noise. Hence, for the OFDM signaling scheme, estimation method that resolves both the remainder and the folding error for range and velocity is needed.

In this work, we extend our prior work on radar OFDM modulation [8], [9] and addresses the problem of estimation of range and velocity of a radar target and OFDM waveform design. The contribution of our work is threefold. First, we propose a two stage estimation method to estimate the fractional components and the folding integers of range and velocity, respectively, using OFDM waveforms. In the first stage, we employ the maximum likelihood approach to estimating the fractional components of the target parameters. In the second stage, the robust Chinese Remainder theorem is utilized to extract folding integers in parameter estimation. For this purpose we present a design of variable frequency step in the OFDM signaling for facilitating robust phase unwrapping. Second, we derive the Cramer-Rao lower bounds for the maximum likelihood estimator for range and Doppler and the total error variance for the developed two-stage estimator. Third, the weights of the OFDM symbols are designed by optimizing the error bound of the estimator subject to the constraints on the peak to average power ratio (PARP) and the total transmission energy. Numerical simulations show that the weighted OFDM scheme improves the Cramer-Rao bound on the range estimation accuracy while controlling the maximum level of PAPR. Hence, the weighted OFDM modulation method provides a flexible modulation mechanism for radar with an improved range estimation accuracy. A provisional patent on this technology has been filed to the US Patent and Trademark Office [10].

Accomplishment 3: Waveform Encoding for Nonlinear Electromagnetic Tomographic Imaging

Electromagnetic (EM) tomographic imaging is an inverse scattering problem which has a wide range of applications in medical imaging, geophysical exploration, nondestructive testing, and target identifications. In EM tomographic imaging, source antennas transmit EM signals into a medium under test and receive scattering signals. Based on the underlying Maxwell's equations, inversion methods are employed to reconstruct a spatial distribution of material parameters such as the dielectric permittivity and/or magnetic permeability of the target and the surrounding medium, thus turning recorded scattering data into images.

The imaging problem is formulated mathematically as a nonlinear optimization problem that seeks to minimize a misfit function between the measured sensor data and a pre-determined model conditioned on parameters which are to be reconstructed. An iterative gradient-descent algorithm is developed to solve the inverse operator (also called the adjoint operator) problem. What it means that the image (i.e., the spatial distribution of the material property values) to be reconstructed is to be updated iteratively until a stopping criteria is reached. We call this method the propagation and backpropagation (PBP) method. To be more specific, the propagation step is to calculate a predicted value of the wave field data from a forward model, while the backpropagation step is to update the image value through the use of adjoint method. For iterative algorithms, slow convergence and high computational complexity are the limiting factors for real-time applications.

In this work, we will address this issue by means of dimensionality reduction through multiple source waveform encoding. Typical full wave tomographic imaging operates in a single-input multiple-output (SIMO) configuration. An image is reconstructed from measured data in response to a single excitation antenna source. The reconstruction process continues till all the sources are excited. For large-scale imaging such as seismic exploration, the number of EM sources is very large. Not only the computational cost is high, the operational expenditures of each data collection process is also significant. In this case, multiple source excitation becomes appealing. For example, in seismic imaging, multiple sources are excited simultaneously to form a so-called supershot to probe the imaging field [11], which means the imaging configuration becomes multiple-input multiple-output (MIMO). The recorded data are processed to form an image. The image is updated when new measurement data is available. This procedure is repeated until the image converges or a predetermined stopping criterion is met. However, multiple wave simultaneous excitation induces cross-talk noise due to wave interference, which, if not treated, will cause image artifacts. Therefore, signal processing techniques such as waveform encoding are needed to mitigate cross-talk noise in the image in order to achieve high quality imaging while reducing the computational complexity. The contribution of our work is threefold. First, we develop three different waveform encoding techniques, i.e., random phase encoding, waveform delay encoding, and uniform weight encoding for the full-wave EM imaging problem. We show that the random phase encoding method results in constant-envelop waveforms and produces the best performance in terms of convergence. Second, this paper extends our early work on microwave imaging in a SIMO configuration [12]. We show that using simultaneous sources made of superposition of encoded sources is able to accelerate iterative algorithms for electromagnetic full-wave inversion, thus demonstrating the effectiveness of waveform encoding, a common signal processing technique, to improve computational efficiency of classic nonlinear inverse problems. Third, although waveform encoding techniques have been studied for acoustical wave imaging (see our early work on MIMO ultrasonic imaging [13], [14]), there is still a lack of research for EM full-wave imaging in applications where the use of EM wave energy is critical. In this work, we develop iterative algorithms that solve time domain Maxwell's equations with coupled electric fields and magnetic fields using waveform encoded excitations and demonstrate faster convergence compared with our prior SIMO imaging algorithm in [12]. The results have been submitted to the 2015 IEEE Global Conference on Signal & Information Processing (see Ref. [15])

In summary, during this project period, we have addressed successfully the overarching technical problem of the project in three aspects, i.e., multi-parameter estimation in cognitive radar, OFDM modulation design for range and Doppler estimation, and waveform encoding for microwave imaging. Our research has led to two top-tier IEEE journal publications (see Ref. [16],

[17]), one peer-reviewed primary conference publication (see Ref. [5]), one conference submission (see Ref. [15]), and three other journal submissions (see Ref. [6], [18], [19]). A provisional patent is also filed to the US Patent and Trademark Office in May 2015 (see Ref. [10]).

References

[1] S. Haykin, “Cognitive radar: a way of the future,” IEEE Signal Processing Magazine, vol. 23, no. 1, pp. 30–40, January 2006.
[2] A. Turlapaty and Y. Jin, “Parameter estimation and waveform design for cognitive radar by minimal free-energy principle,” in IEEE International Conference on Acoustics, Speech and Signal Processing, May 2013, pp. 6244–6248.
[3] K. Friston, “The free-energy principle: a unified brain theory,” Nature Reviews Neuroscience, vol. 11, pp. 127 - 138, February 2010.
[4] V. Smidl and A. Quinn, “Variational Bayesian filtering,” IEEE Transactions on Signal Processing, vol. 56, no. 10, pp. 5020–5030, October 2008.
[5] A. Turlapaty and Y. Jin, “Multi-parameter estimation for cognitive radar in compound Gaussian clutter”, IEEE International Conference on Acoustics, Speech and Signal Processing (ICASSP), Brisbane, Australia, April 19-24, 2015
[6] A. Turlapaty and Y. Jin, “Multi-Parameter Estimation in Compound Gaussian Radar Clutter by Free-Energy Principle”, (submitted for publication)
[7] S. Sen and A. Nehorai, “Adaptive OFDM radar for target detection in multipath scenarios,” IEEE Transactions on Signal Processing, vol. 59, no. 1, pp. 78–90, January 2011.
[8] A. Turlapaty, Y. Jin, and Y. Xu, “Range and velocity estimation of radar targets by weighted OFDM modulation,” in Proceedings of IEEE Radar Conference. May 2014, pp. 1358 – 1362, IEEE
[9] A. Turlapaty and Y. Jin, “Waveform design for coexistence of radar and communication systems,” in Proceedings of IEEE Radar Conference. May 2014, pp. 315 – 319, IEEE.
[10] A. Turlapaty, Y. Jin, Y. Xu, “Weighted OFDM modulation technology for radar parameter estimation”, Provisional patent application no. 62/162962, May 2015.
[11] J. Godwin and P. Sava, “CWP-645 Simultaneous source imaging by amplitude encoding,” Colorado School of Mines.
[12] C. Dong, Y. Jin and E. Lu, “Time Domain Electromagnetic Tomography Using Propagation and Backpropagation Method”, IEEE International Conference on Image Processing (ICIP) 2012, Orlando, FL, October 2012, pp. 2081-2084, IEEE.
[13] C. Dong and Y. Jin, “MIMO Nonlinear Ultrasonic Tomography by Propagation and Backpropagation Method”, IEEE Transactions on Image Processing, vol. 22, no. 3, pp. 1056-1069, March 2013.
[14] C. Dong, Y. Jin, and E. Lu, “Accelerated nonlinear multichannel ultrasonic tomographic imaging using target sparseness”, IEEE Transactions on Image Processing, vol. 23, no. 3, pp. 1379-1393, March 2014.
[15] Y. Jin, C. Dong, and E. Lu, “Waveform Encoding for Nonlinear Electromagnetic Tomographic Imaging”, submitted to IEEE Global Conference on Signal & Information Processing 2015.
[16] M. Yu, D. Zhao, Y. Jin, and B. Wang, “Near-Field Image Restoration for Rotman Lens by Localized Angle-Time Spread Function Based Filtering Method”, IEEE Transactions on Antennas and Propagation, vol. 63, no. 5, pp. 2353 – 2358, May 2015.
[17] A. Turlapaty and Y. Jin, “Bayesian Sequential Parameter Estimation by Cognitive Radar with Multi-Antenna Arrays”, IEEE Transactions on Signal Processing, vol. 63, no. 4, pp. 974-987, February 2015.
[18] A. Turlapaty and Y. Jin, “Weighted OFDM modulation for range and velocity estimation of radar targets”, (submitted for publication)
[19] F. Foroozan, A. Asif, and Y. Jin, “Cramer-Rao Bound Improvement in Angle-Velocity Estimation with the Time Reversal MIMO Radar”, (submitted for publication)

Technology Transfer

Final Report
Grant Number: W911NF-11-1-0160
Reporting Period: May 9, 2014 - May 8, 2015

Title: Sparsity Aware Radar Sensor Imaging in Complex Scattering Environments

Yuanwei Jin
Department of Engineering and Aviation Sciences
University of Maryland Eastern Shore
Email: yjin@umes.edu

June 5, 2015

Abstract

Radar imaging and parameter estimation can be modeled as an inverse problem: $\mathbf{y} = \mathbf{R} \cdot \mathbf{f} + \mathbf{w}$, i.e., from noisy measurement vector $\mathbf{y}$ to reconstruct or estimate the target parameter vector $\mathbf{f}$, which could be the spatial reflectivity coefficient vector or other target properties. The operator $\mathbf{R}$ (linear or nonlinear) depends on many factors such as the waveform transmission strategy, the data collection geometry, the medium property, and the underlying wave propagation models. A fundamental question that this project aims to address is: how to explore novel waveform transmission, modulation, a priori knowledge of target, and statistical computing techniques to achieve superior imaging and parameter estimation.

The main accomplishments of the project during this reporting period are: (1) The development of multi-parameter estimation methods for cognitive radar under compound Gaussian clutter using variational Bayesian inference; 2) The development of range and Doppler estimation method using weighted OFDM modulation; and 3) The development of novel microwave nonlinear image reconstruction algorithm using waveform encoding schemes.

Contents

Chapter 1

Multi-Parameter Estimation by Variational Bayesian

1.1 Introduction

Cognitive radar has been proposed as a fully adaptive radar transmission and reception system in [Haykin, 2006]. In cognitive radar, both the transmitter and the receiver parameters are estimated and updated by learning from the unknown environment, forming a belief on what is learned, and propagating this belief by Bayesian inference. From the parameter estimation perspective, the Bayesian approach enables inclusion of prior information (knowledge) of radar target and clutter by estimating the posterior density of the unknown parameters. The estimation is optimal in the sense of minimizing the Bayesian mean squared error (MSE). Typically, the full joint probability density function (pdf) of all the parameters of interest including the nuisance parameters is considered. However, in the case of high-dimensional multi-variate integration of Bayesian posterior density, the calculation of the posterior pdf and its marginal can be computationally prohibitive and tractable analytical solutions are often not available. Furthermore, the estimation accuracy is directly related to the number of data samples in the Bayesian estimator. However, in many radar applications, the number of available data samples is limited. These computational challenges and limitations must be addressed to develop cognitive radar.

In [Turlapaty and Jin, 2013], we proposed a variational Bayesian (VB) based method for parameter estimation and waveform design where a single parameter estimation problem is considered. Variational Bayesian aims to minimize free energy (FE) [Friston, 2010, Turlapaty and Jin, 2013], which is equivalent to minimizing the Kullback-Liebler divergence between the true density and an approximation density. As a result of this functional optimization for density estimation, the marginal VB posterior density has an explicit functional structure, thus leading to closed form solutions [Smidl and Quinn, 2008]. This work extends our prior work in [Turlapaty and Jin, 2013] to multiple parameter estimation in the context of cognitive radar. In adaptive radar detection, estimating the clutter covariance matrix is a very important task since the detection performance depends directly on the accuracy of the estimate. For example, in high-resolution and low-grazing-angle radar, only a small sea surface area is illuminated by a narrow radar beam. The sea clutter due to reflection from the small patch of sea surface is random and non-stationary [Sangston and Gerlach, 1994], which is commonly modeled as a compound-Gaussian distribution to characterize its heavy-tailed clutter distributions [Wright, 1968, Greco et al., 2004]. Hence, the Bayesian estimator must consider a multi-parameter estimation problem by which the parameters in the compound-Gaussian model, the radar target response, as well as other nuisance parameters are estimated. In this work,

we compare the performance of the proposed VB method with the expectation-maximization (EM) algorithm. In the EM method, expectations of sufficient statistics are computed with respect to the posterior density of hidden variables and then used to iteratively estimate the unknown parameters by the maximum likelihood principle [Candy, 2009, Wang et al., 2006]. We show in this work that the variational algorithms outperform the EM method particularly when estimating parameters that follow non-Gaussian nonlinear models in Bayesian inference. Hence, the proposed variational algorithms provide appealing computational advantages for cognitive radar.

1.2 Problem Formulation

1.2.1 Radar signal model

The compound clutter model is a product of two random processes [Wang et al., 2006, Wright, 1968, Greco et al., 2004],

$$\psi_t = \sqrt{u_t} w_t \tag{1.1}$$

where the speckle w_t characterizing the local scattering and is modeled as a zero mean complex Gaussian (ZMCG) process $w_t \sim \mathcal{CN}(0, \sigma^2)$. The component u_t is a slow changing process termed texture that follows an inverse Gamma distribution $u_t \sim \Gamma^{-1}(\alpha)$, where the pdf of u_t is

$$p(u_t; \alpha) = \frac{\alpha^\alpha}{\Gamma(\alpha)} u_t^{-\alpha-1} \exp\left(-\frac{\alpha}{u_t}\right) \tag{1.2}$$

The model (1.1) is referred to as K-clutter [Gini et al., 2000, Sangston and Gerlach, 1994] and the parameter α is known as the Nakagami parameter [Haykin et al., 2002]. Next, we assume the radar transmits a waveform Φ_t and the electromagnetic (EM) energy hits a target with a complex amplitude response x. The reflected EM energy is intercepted by the radar receiver. The radar signal model that includes the clutter from (1.1) is given by

$$y_t = \Phi_t x + \psi_t, \;\; t = 1, 2, \cdots, N \tag{1.3}$$

The conditional probabilistic model of the measurements is a complex Gaussian distribution given by

$$y_t | u_t, x, \sigma^2 \sim \mathcal{CN}(\Phi_t x, u_t \sigma^2) \tag{1.4}$$

1.2.2 Problem of parameter estimation

The complete hierarchical stochastic model, i.e., the joint probability density function of the measurements, hidden variables, and the unknown parameters at time t is given by

$$p(y_t, u_t, x, \sigma^2, \alpha; \Phi_t) \;\; = \;\; p(y_t | u_t, x, \sigma^2; \Phi_t) p_0(x, \sigma^2) p(u_t | \alpha) p_0(\alpha) \tag{1.5}$$

where $p(y_t | u_t, x, \sigma^2; \Phi_t)$ is the conditional density given in (1.4). The probabilistic model of texture $p(u_t|a)$ is given by (1.2). $p_0(x, \sigma^2)$ and $p_0(\alpha)$ are prior densities of (x, σ^2) and α, respectively. Initially, the unknown parameter vector is given by $[x, \sigma^2, \alpha]$. When we use a variational estimation method, the covariance estimate depends on the current estimate of α. However, initially this mutual dependence of estimates introduces a multiplicative error in the estimates of these two parameters. To correct this error, we use the technique of covariance adjustment and introduce an additional parameter λ in the texture model (1.2) by redefining the covariance in terms of an adjusted covariance

σ_a^2, [Wang et al., 2006], i.e., the relation between the actual covariance and the adjusted covariance is $\sigma^2 = \sigma_a^2/\lambda$. Hence, the adjusted texture model becomes

$$p(u_t|\alpha,\lambda) = (\alpha\lambda)^\alpha/\Gamma(\alpha)\, u_t^{-\alpha-1} e^{-\alpha/(\lambda u_t)} \tag{1.6}$$

The new augmented parameter vector to be estimated is

$$\boldsymbol{\theta} = [x, \sigma^2, \alpha, \lambda] \tag{1.7}$$

1.3 Variational Bayesian Estimator

1.3.1 Background of variational Bayesian inference

Consider a hierarchical probabilistic model

$$p(\mathbf{Y}, \mathbf{X}, \boldsymbol{\theta}) = p(\mathbf{Y}|\mathbf{X}, \boldsymbol{\theta}) p(\mathbf{X}|\boldsymbol{\theta}) p(\boldsymbol{\theta}) \tag{1.8}$$

where $\mathbf{Y}$ are the measurements, $\mathbf{X}$ are hidden variables, and $\boldsymbol{\theta}$ are unknown parameters. In the exact Bayesian approach, the unknown parameters are determined by evaluating the joint posterior density $p(\mathbf{X}, \boldsymbol{\theta}|\mathbf{Y})$ using the Bayes rule

$$p(\mathbf{X}, \boldsymbol{\theta}|\mathbf{Y}) = p(\mathbf{Y}, \mathbf{X}, \boldsymbol{\theta})/p(\mathbf{Y}) \tag{1.9}$$

while the marginal posterior $p(\boldsymbol{\theta}|\mathbf{Y})$ is evaluated by integrating $\mathbf{X}$ out from the joint posterior. However, in practice the denominator in (1.9) is usually theoretically intractable except in some special cases. Moreover, in the case of multiple parameters in $\boldsymbol{\theta}$ even the numerical integration is computationally expensive and time consuming [Smidl and Quinn, 2008]. To address this issue, approximation methods are needed to determine alternative density functions. Variational Bayesian estimation aims to find approximations $q(\mathbf{X})$ and $q(\boldsymbol{\theta})$ to the marginal posterior densities of parameters that minimize the variational free energy of the approximate density and the joint pdf in (1.8) [Beal and Ghahramani, 2003]. So the key idea is factorization of $q(\mathbf{X}, \boldsymbol{\theta})$ into $q(\mathbf{X})q(\boldsymbol{\theta})$, thus separating the densities of $\mathbf{X}$ and $\boldsymbol{\theta}$. The variational free energy (FE) for $\mathbf{Y}, \mathbf{X}$ and $\boldsymbol{\theta}$ is given by [Turlapaty and Jin, 2013, Smidl and Quinn, 2008, Friston, 2010]

$$F(\mathbf{Y}, \mathbf{X}, \boldsymbol{\theta}) = -\int q(\mathbf{X}) q(\boldsymbol{\theta}) \log \frac{p(\mathbf{Y}, \mathbf{X}, \boldsymbol{\theta})}{q(\mathbf{X}) q(\boldsymbol{\theta})} d\mathbf{X} d\boldsymbol{\theta} \tag{1.10}$$

The approximate density $q(X)$ of hidden variables is determined by variational Bayesian expectation (VBE)

$$q(\mathbf{X}) = \arg\min_{q(\mathbf{X})} F(\mathbf{Y}, \mathbf{X}, \boldsymbol{\theta}) \tag{1.11}$$

where the optimal solution to (1.11) is given by

$$\log q(\mathbf{X}) = \langle \log p(\mathbf{X}|\boldsymbol{\theta}) \rangle_{q(\boldsymbol{\theta})} + \langle \log p(Y|X, \boldsymbol{\theta}) \rangle_{q(\boldsymbol{\theta})} + \text{const.} \tag{1.12}$$

where $\langle \cdot \rangle$ is an inner product. The approximate density $q(\boldsymbol{\theta})$ of the parameters is determined by variational Bayesian minimization (VBM)

$$q(\boldsymbol{\theta}) = \arg\min_{q(\boldsymbol{\theta})} F(\mathbf{Y}, \mathbf{X}, \boldsymbol{\theta}) \tag{1.13}$$

where the optimal solution to (1.13) is given by [Paisley et al., 2012, Tzikas et al., 2008]

$$\log q(\boldsymbol{\theta}) = \log p_0(\boldsymbol{\theta}) + \langle \log p(Y|X, \boldsymbol{\theta}) \rangle_{q(\mathbf{X})} + \text{const.} \tag{1.14}$$

1.3.2 Variational Bayesian estimator

The new joint probability density function depends on the measurement vector $\mathbf{Y} = [y_1, \cdots, y_N]^T$, the vector of independent hidden variables $\mathbf{U} = [u_1, \cdots, u_N]^T$, and the adjusted parameter vector $\boldsymbol{\theta}$, which takes the form of

$$p(y_t, u_t, x, \sigma^2, \alpha, \lambda; \Phi_t) \;\; = \;\; p(y_t|u_t, x, \sigma^2; \Phi_t) p_0(x, \sigma^2) p(u_t|\alpha, \lambda) p_0(\alpha, \lambda) \tag{1.15}$$

The full data log-likelihood function is given by

$$\Lambda(\mathbf{Y}, \mathbf{U}, \boldsymbol{\theta}) = \sum_t \log p(y_t|u_t, x, \sigma^2; \Phi_t) + \sum_t \log p(u_t|\alpha, \lambda) + \log p_0(x, \sigma^2) + \log p_0(\alpha, \lambda) \tag{1.16}$$

Eqn. (1.16) involves six parameters, which is very complicated. Next, we present a variation Bayesian approach to approximate it in the sense of minimization of the free-energy (i.e., KL divergence, [Turlapaty and Jin, 2013]), so that analytically trackable closed form expressions of pdfs can be obtained. The evaluation of (1.16) involves the expectation and minimization steps (i.e., E-step and M-step) while using the VB approach. Due to space limitations, we will omit some details of the mathematical derivation.

VB estimation step (VBE)

The first step in variational estimation is to determine the approximate density of the hidden variable u_t given the measurements y_t by using the minimum free energy principle. Since the hidden variables u_t are independent across time, the approximate density of the vector $\mathbf{U}$ can be written as $q(\mathbf{U}) = \prod_{t=1}^{N} q(u_t)$. Its approximate density will be obtained by minimizing the free-energy defined in (1.10), which can be re-written as

$$F(\mathbf{Y}, \mathbf{U}, \boldsymbol{\theta}) = -\Big\langle \Lambda(\mathbf{Y}, \mathbf{U}, \boldsymbol{\theta}) \Big\rangle_{q(\mathbf{U})} + \Big\langle \sum_{t=1}^{N} \log(q(u_t)) \Big\rangle_{q(\mathbf{U})}$$

based upon (1.16). Hence, the optimization problem is given by

$$q(u_t) = \arg\min_{q(u_t)} F(\mathbf{Y}, \mathbf{U}, \boldsymbol{\theta}) \tag{1.17}$$

Following the optimal solution in (1.12), we obtain

$$\log q(u_t) = \langle \log p(u_t|\alpha, \lambda) \rangle_{q(\alpha,\lambda)} + \langle \log p(y_t|u_t, x, \sigma^2) \rangle_{q(x,\sigma^2)} + \text{const.} \tag{1.18}$$

Next, inserting the pdf (1.4) in (1.18), we have

$$q(u_t) \propto u_t^{-\left(\langle \alpha \rangle_{q(\alpha,\lambda)} + 1\right) - 1} e^{-\left[\langle \alpha/\lambda \rangle_{q(\alpha,\lambda)} + \langle |y_t - \Phi_t x|^2 \frac{1}{\sigma^2} \rangle_{q(x,\sigma^2)}\right]/u_t} \tag{1.19}$$

which is consistent with the definition of an inverse Gamma density function $\Gamma^{-1}(\cdot)$, leading to a closed form $q(u_t) = \Gamma^{-1}\Big(u_t; c_U, d_U\Big)$ with its parameters being $c_U = \langle \alpha \rangle_{q(\alpha,\lambda)} + 1$ and $d_U = \langle \alpha/\lambda \rangle_{q(\alpha,\lambda)} + \langle |y_t - \Phi_t x|^2/\sigma^2 \rangle_{q(x,\sigma^2)}$.

VB minimization step (VBM)

The optimization problem for estimating the pdf of the parameter vector $\boldsymbol{\theta}$ is given by

$$q(x, \sigma^2, \alpha, \lambda) = \arg \min_{q(x,\sigma^2,\alpha,\lambda)} F(\mathbf{Y}, \mathbf{U}, \boldsymbol{\theta}) \tag{1.20}$$

We write the variational posterior density of the parameter vector in (1.14) as follows

$$\begin{aligned} \log q(x, \sigma_a^2, \alpha, \lambda) \;=\; & \log p_0(\alpha, \lambda) + \log p_0(x, \sigma_a^2) + \sum_{t=1}^{N} \big\langle \log p(y_t|u_t, x, \sigma_a^2; \Phi_t) \big\rangle_{q(u_t)} + \\ & \sum_{t=1}^{N} \big\langle \log p(u_t|\alpha, \lambda) \big\rangle_{q(u_t)} + \text{const.} \end{aligned} \tag{1.21}$$

Note that the terms for the joint pdf of (x, σ_a^2) are separable from the pdf of (α, λ), i.e.,

$$q(x, \sigma_a^2, \alpha, \lambda) = q(x, \sigma_a^2)\; q(\alpha, \lambda) \tag{1.22}$$

Next, we evaluate $\log q(x, \sigma_a^2)$ and $\log q(\alpha, \lambda)$ from (1.21) and (1.22) to derive approximate closed forms. We start by writing the log-function of pdf of (x, σ_a^2) as

$$\begin{aligned} \log q(x, \sigma_a^2) = \log p_0(x, \sigma_a^2) + & \sum_{t=1}^{N} \Big\langle \log 1/(\pi u_t \sigma_a^2) \Big\rangle_{q(u_t)} \\ & - \sum_{t=1}^{N} \Big\langle |y_t - \Phi_t x|^2/(u_t \sigma_a^2) \Big\rangle_{q(u_t)} + \text{const.} \end{aligned} \tag{1.23}$$

which leads to the joint pdf $q(x, \sigma_a^2)$, which is a complex Gaussian inverse Gamma ($\mathcal{CGIG}$) distribution

$$q(x, \sigma_a^2) \quad \propto \quad p_0(x, \sigma_a^2)(1/\sigma_a^2)^N e^{-\sum_{t=1}^{N} |y_t - \Phi_t x|^2/\sigma_a^2 \langle 1/u_t \rangle_{q(u_t)}} \tag{1.24}$$

Note that the functional form is nicely preserved if the prior pdf is assumed to be $p_0(x, \sigma_a^2) \sim \mathcal{CGIG}(\rho, \eta, \beta, \mu_x)$, which leads to an explicit single $\mathcal{CGIG}$ distribution expression for $q(x, \sigma_a^2)$. Next, we examine the logarithm of the joint pdf of (α, λ), which is given by (where C is a constant)

$$\log q(\alpha, \lambda) = \log p_0(\alpha, \lambda) + \sum_{t=1}^{N} \langle \log p(u_t|\alpha, \lambda) \rangle_{q(u_t)} + C \tag{1.25}$$

By (1.6) and $T_l \triangleq \sum_{t=1}^{N} \langle \log u_t \rangle_{q(u_t)}$, $T_i \triangleq \sum_{t=1}^{N} \langle 1/u_t \rangle_{q(u_t)}$, we obtain the joint pdf $q(\alpha, \lambda)$ as follows

$$q(\alpha, \lambda) \propto p_0(\alpha, \lambda) \frac{(\frac{\alpha}{\lambda})^{N\alpha}}{(\Gamma(\alpha))^N} e^{-\alpha(T_l + T_i/\lambda)} \tag{1.26}$$

Since this is not a known probability distribution, it can not provide closed form solutions. We can rely on numerical means for calculation, or alternatively, we propose to induce another layer of factorization on the joint pdf $q(\alpha, \lambda)$ as

$$q(\alpha, \lambda) = q(\alpha) q(\lambda) \tag{1.27}$$

via the optimization problem to obtain closed form expressions of $q(\alpha)$ and $q(\lambda)$, i.e.,

$$\arg \min_{q(\alpha),q(\lambda)} F(\mathbf{Y}, \mathbf{U}, x, \sigma^2, \alpha, \lambda) \tag{1.28}$$

where the new free-energy quantity is defined by

$$\begin{aligned} F(\mathbf{Y}, \mathbf{U}, x, \sigma^2, \alpha, \lambda) &= -\Big\langle \Lambda(\mathbf{Y}, \mathbf{U}, x, \sigma_a^2, \alpha, \lambda) \Big\rangle_{q(\alpha)q(\lambda)q(\mathbf{x},\sigma^2)q(\mathbf{U})} \\ &\quad + \Big\langle q(\alpha)q(\lambda)q(\mathbf{x},\sigma^2)q(\mathbf{U}) \Big\rangle_{q(\alpha)q(\lambda)q(\mathbf{x},\sigma^2)q(\mathbf{U})} \end{aligned}$$

As a result, we obtain the approximate inverse Gamma distribution for $q(\lambda) = \Gamma^{-1}(\lambda; c_\lambda, d_\lambda)$ and the approximate Gamma distribution for $q(\alpha) = \Gamma(c_\alpha(0), d_\alpha(0))$ by Lindley's approximation [Lindley, 1980]. Due to space limitations, we will omit the detailed expressions of $q(\alpha)$ and $q(\lambda)$ in this work.

1.4 Numerical Simulations

We present estimation performance of the three estimators by numerical simulations. The three estimators are: **(1) VBN-PF:** Variational Bayesian approach with induced factorization on $q(\alpha, \lambda)$ and a numerical integration for evaluation of the moments of α. **(2) VBL-PF:** Variational Bayesian approach with induced factorization on $q(\alpha, \lambda)$ and the Lindley's approximation for evaluation of moments of α [Lindley, 1980]. **(3) PXEM:** parameter expanded expectation maximization approach, where $q(u_t)$ is updated based on Bayesian approach, while each of the unknown parameters is determined by using the maximum likelihood principle [Wang et al., 2006]. The key differences between the EM and VB algorithms are twofold. First, in the EM method, unknown parameters are considered as deterministic values and estimated using the maximum likelihood (ML) method whereas in the VB method the unknown parameters are modeled as random variables and the Bayesian approach is used to determine their approximate posterior densities. Second, in the EM method, each M-step only receives the updated sufficient statistics from the E-step, where as in VB, as a result of the Bayesian principle, the VBM step utilizes the updated priors of the randomized parameters.

The parameters of the clutter model and target model are chosen as follows: Nakagami parameter $\alpha = 3$, clutter power $\sigma_a^2 = 5$ dB, the complex target response $x = 1.6 + 1.0i$, the spectral density of the waveform is normalized $|\Phi_t| = 1$, the number of observations N varies from 10 to 1000.

Figs. 1.1(a) shows that, for the parameters σ^2, the variational algorithm VBL-PF outperforms the PXEM algorithm when the number of observations $N < 200$ while the VBN-PF method outperforms the PXEM for all values of N. For the estimation of Nakagami parameter α, the performance of VB methods is much better than PXEM in terms of MSE, as shown in Fig. 1.1(b). This is because in the PXEM method, the ML solution is obtained by solving a nonlinear equation due to the non-Gaussian clutter model. For the estimation of radar target response x, the three methods have very similar performance for all values of N as depicted in Fig. 1.1(c). The explanation for the similarity is that the unknown parameter is a linear function of the observations and follows a Gaussian distribution. Note that ML and Bayesian algorithms usually have similar performance for Gaussian linear models. The advantage of VB approach can be observed for non-Gaussian nonlinear models such as the ones that involve σ^2 and α. This observation is consistent with existing literature on variational Bayesian studies [Smidl and Quinn, 2008, Tzikas et al., 2008]. Finally, The estimation performance of the adjustment parameter λ is not discussed as it is only a nuisance parameter for correcting the multiplicative error.

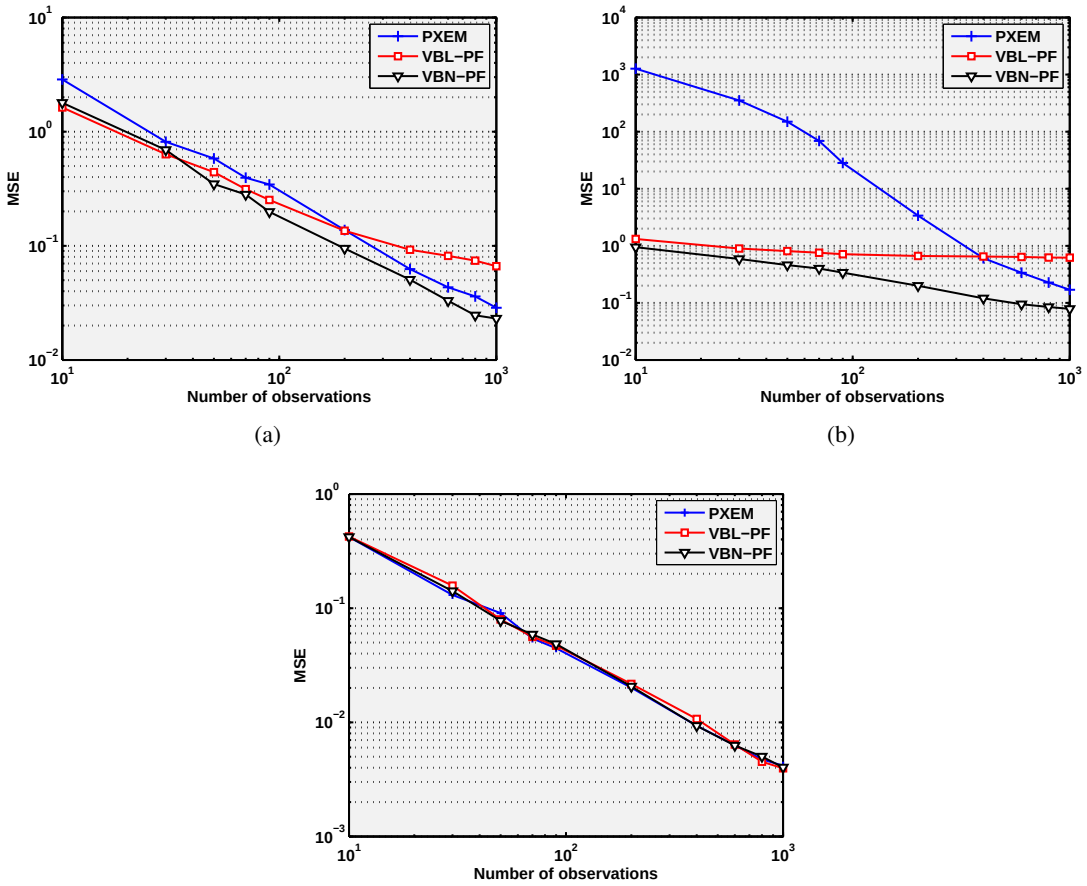

Figure 1.1: Comparison of mean squared error (MSE) between PXEM, VBN-PF and VBL-PF. (a) clutter noise variance σ^2, (b) Nakagami parameter α, and (c) target response x.

1.5 Conclusion

We develop variational Bayesian algorithms for estimating multi-parameters of a compound Gaussian clutter model and target response. The VB method yields closed form expressions for the posterior probability density functions and results in improved estimation performance for the clutter model, especially for parameters of non-Gaussian nonlinear models and when the number of measurements is small.

Chapter 2

Range and Doppler Estimation by Weighted OFDM Modulation

.

2.1 Introduction

An increasing array of technologies in communications services has resulted in scarcity of the frequency spectrum. Spectrum congestion becomes a growing problem, thus limiting the operational capabilities of competing wireless systems due to mutual interference. The call for spectrum sharing is to allow co-existence between various RF systems including Wi-Fi, cellular system, and S-band radar that operate in the same or close frequency band while achieving normal operational performance levels. Traditionally, fixed spectrum allocation has been used to prevent interference for radar and communications systems that operate in close ranges. However, with the huge success in wireless connectivity and cellular communication system, more frequency bands are allocated for commercial applications, which makes the fixed spectrum allocation approach increasingly difficult to implement.

One of the alternative approaches to achieve spectrum sharing is to design reconfigurable wireless platforms, for example, a single RF platform that can be used to realize communication and radar functions. However, the intended radar functions are quite different than communications systems. Radar is an active sensing device that relies on transmission waveforms for target detection, estimation, and tracking with the goal of achieving high resolution. For a communications system, information bits transfer is accomplished by waveform modulation and demodulation. The primary goal for communications is spectral efficiency and throughput. Hence, one of the challenges that we face is to design modulation waveforms that can be dual-used for radar and communication. Many different modulation schemes that are traditionally used for communications can also be utilized for radar. For example, spread spectrum techniques have been used in a vehicle-to-vehicle communication and ranging system under a single RF platform [Uchida et al., 1994]. Orthogonal frequency division multiplexing (OFDM) or its variations [Sit et al., 2011] have also been used in radar [Braun et al., 2010].

There are two noticeable advantages of using OFDM modulation. First, by reusing the OFDM waveform, limited extra hardware is needed for optimizing both wireless communication and radar detection. Second, recent research has shown that OFDM offers robustness performance against multipath fading [Sen and Nehorai, 2011, Garmatyuk et al., 2007] in highly mobile environments [Schmidl and Cox, 1997]. Note that constant envelope signaling with phase modulation is gener-

ally preferred for hardware realization [Testi et al., 2013]. However, the constant envelope OFDM waveform (CE-OFDM) has a relatively high peak to average power ratio (PAPR). The upper bound equals to the number of subcarrier frequencies [Ochiai and Imai, 2001]. Hence, the estimation performance is limited by the number of independent individual OFDM symbols.

In this work, we present a non-linear least squares approach to estimate the velocity and range of a radar target based on a weighted OFDM (WOFMD) modulation scheme. The proposed WOFDM method is a non-constant envelop modulation method. The weights of the WOFDM symbols are designed by optimizing the error bound of the estimator subject to the constraints of PARP and a total transmission energy. Numerical simulations show that the weighted OFDM scheme improves the Cramer-Rao lower bound on the range estimation accuracy while controlling the maximum level of PAPR. Hence, this method provides a flexible and reconfigurable realization mechanism for the radar/comm system co-design with an improved estimation range accuracy of radar targets.

2.2 Signal Models

We consider an OFDM signaling system with N subcarriers, each modulated with a data symbol. The time domain transmitted (complex envelop) signal in the m-th pulse $(m = 0, \cdots, M-1)$ can be written as

$$s_m(t) = \sum_{n=0}^{N-1} a_{m,n} e^{j2\pi f_n t} 1_m(t, T_{\text{PRI}}, T_p) \tag{2.1}$$

where the m-th rectangular pulse function is defined as

$$1_m(t, T_{\text{PRI}}, T_p) = \begin{cases} 1 & mT_{\text{PRI}} \le t \le mT_{\text{PRI}} + T_p \\ 0 & mT_{\text{PRI}} + T_p < t < (m+1)T_{\text{PRI}} \end{cases} \tag{2.2}$$

and $a_{m,n}$ denotes the complex weights transmitted over the n-th subcarrier for the m-th modulation symbol. For a constant envelope OFDM modulation method, the following condition

$$\sum_{n=0}^{N-1} |a_{m,n}|^2 = a = \text{const.} \tag{2.3}$$

is imposed. T_{PRI} is the pulse repetition interval (PRI). T_p is the OFDM symbol duration and the subcarrier spacing $\Delta f = \frac{1}{T_p} = B/N$, where B is the signal bandwidth. The individual subcarrier frequency is

$$f_n = \left(f_c - \frac{B}{2}\right) + n\Delta f, \ n = 0, 1, \cdots N-1 \tag{2.4}$$

where f_c is the carrier frequency of the radar. In the presence of a reflecting target at the distance R with the relative velocity of v, the relative Doppler shift is $\beta = \frac{2v}{c}$. Hence, the induced Doppler frequency at the n-th subcarrier is

$$f_n^d = f_n \beta = \left(f_c + \frac{n}{T_p}\right) \frac{2v}{c} \tag{2.5}$$

We assume that the $f_c \gg B$, i.e., the carrier frequency is much larger than the signal bandwidth, hence, it is safe to assume that the Doppler frequency is fixed with respect to the subcarriers, i.e., the average Doppler frequency is

$$f_d \approx f_c \frac{2v}{c} \tag{2.6}$$

thus applying the doppler shift on frequency $f_n \rightarrow f_n + f_d$ and the time delay $t \rightarrow t - \tau$ we have the received signal

$$x_m(t) = \sum_{n=0}^{N-1} a_{m,n} e^{j2\pi(f_n+f_d)(t-\tau)} 1_m(t, T_{\text{PRI}}, T_p) + w_m(t) \tag{2.7}$$

We rewrite (2.7) as

$$x_m(t) = A\, s_m(t-\tau) e^{j2\pi f_d(t-\tau)} + w_m(t) \tag{2.8}$$

where τ is the round trip time delay between the radar and target. A is the target response. Note that in general, the reflection coefficient A is complex and may vary in different subcarrier channels. For simplicity, A is assumed to be a deterministic constant in this work. $w_m(t)$ is the clutter and measurement noise, following a zero mean complex Gaussian distribution. Inserting (2.1), (2.4) and (2.6) to (2.8), we obtain

$$x_m(t) = x_m^s(t) 1_m(t, T_{\text{PRI}}, T_p) + w_m(t) \tag{2.9}$$

where the signal component is

$$x_m^s(t) \;=\; A \sum_{n=0}^{N-1} a_{m,n} e^{j2\pi(n\Delta f(t-\tau) - f_c\tau)} e^{j2\pi f_d(t-\tau)} e^{j2\pi f_c t}$$

The corresponding baseband (complex envelope) signal is

$$\begin{aligned} y_m(t) &= x_m^s(t) 1_m(t, T_{\text{PRI}}, T_p) e^{-j2\pi f_c t} + w_m(t) && (2.10)\\ &= \sum_{n=0}^{N-1} A\, a_{m,n} e^{j2\pi(n\Delta f(t-\tau) - f_c\tau)} e^{j2\pi f_d(t-\tau)} 1_m(t, T_{\text{PRI}}, T_p) + w_m(t) && (2.11) \end{aligned}$$

Note that, for an OFDM system, the sampling interval T_s is typically chosen such that $\Delta f T_s = 1/N$. Hence, the sampled version of $y_m(l)$ with $(l = 0, \cdots, N-1)$ becomes

$$y_m(l) = A \sum_{n=0}^{N-1} a_{m,n} e^{j2\pi \frac{n}{N} l} e^{-j2\pi(n\Delta f + f_c)\tau} \times e^{j2\pi f_d(T_s(l+mQN)-\tau)} + w_m(l) \tag{2.12}$$

where $Q = T_{\text{PRI}}/T_p$. Next, we define

$$Y_{m,n}^s \triangleq A\, a_{m,n} e^{-j2\pi(n\Delta f + f_c)\tau} e^{j2\pi f_d(T_s mQN)} \tag{2.13}$$

Using the definition of inverse DFT and $T_s = \frac{1}{N\Delta f}$ we can re-write (2.12) as

$$y_m(l) = N\{\text{IDFT}\left[Y_{m,n}^s\right]\} e^{j2\pi \frac{f_d}{\Delta f}\frac{l}{N}} e^{-j2\pi f_d\tau} + w_m(l) \tag{2.14}$$

the term $e^{j2\pi \frac{f_d}{\Delta f}\frac{l}{N}}$ amounts to modulation in the time domain. Hence the DFT of $y_m(l)$ has a corresponding frequency shift $\frac{f_d}{\Delta f}$. Thus, applying DFT on (2.14) implies

$$Y'_{m,n} = N Y^s_{m,n-\frac{f_d}{\Delta f}}\, e^{-j2\pi f_d\tau} + W_{m,n} \tag{2.15}$$

In radar estimation, we can assume that $f_d \leq \Delta f$ thus the only term that is influenced by modulation is $e^{-j2\pi(n\Delta f + f_c)\tau}$ with $n = n - \frac{f_d}{\Delta f}$ and

$$Y'_{m,n} = NA\, a_{m,n} e^{-j2\pi((n-\frac{f_d}{\Delta f})\Delta f + f_c)\tau} e^{j2\pi f_d(T_s mQN)} \times e^{-j2\pi f_d\tau} + W_{m,n} \tag{2.16}$$

which can be simplified as

$$Y'_{m,n} = A' a_{m,n} e^{j2\pi(m f_d T_s Q N - n\Delta f \tau)} + W_{m,n} \tag{2.17}$$

where $A' = ANe^{-j2\pi f_c \tau}$ and is invariant term respect to m and n. $W_{m,n}$ is the DFT of the noise term $w_m(l)$. Dividing the known OFDM symbols $a_{m,n}$ on both sides of (2.17), we obtain,

$$Y_{m,n} = A' e^{j2\pi(m f_d T_s Q N - n\Delta f \tau)} + W^a_{m,n} \tag{2.18}$$

where $Y_{m,n} = \frac{Y'_{m,n}}{a_{m,n}}$ and $W^a_{m,n} = \frac{W_{m,n}}{a_{m,n}}$.

2.3 Minimum Nonlinear Least-Squares Estimator

We let $A' = be^{j\phi_A}$ be the target response with b and ϕ_A being the magnitude and phase of target response. The parameter vector of interest is

$$\boldsymbol{\theta} = [b, \phi_A, f_d, \tau] \tag{2.19}$$

From the signal model (2.18), the nonlinear least-squares error function is,

$$\begin{aligned} L_n(Y;\boldsymbol{\theta}) &= \sum_{m=0}^{M-1}\sum_{n=0}^{N-1} |W^a_{m,n}|^2 \\ &= \sum_{m=0}^{M-1}\sum_{n=0}^{N-1} |Y_{m,n} - be^{j\phi_A} e^{j2\pi(m f_d T_s Q N - n\Delta f \tau)}|^2 \end{aligned} \tag{2.20}$$

where M is the number of pulses in the coherent processing interval. Hence, we obtain

$$L_n(Y;\boldsymbol{\theta}) = \sum_{m=0}^{M-1}\sum_{n=0}^{N-1} \Big(|Y_{m,n}|^2 + b^2 - 2\Re\{ Y^*_{m,n} be^{j\phi_A} e^{j2\pi(m f_d T_s Q N - n\Delta f \tau)} \} \Big) \tag{2.21}$$

The parameters $\boldsymbol{\theta}$ can be determined by minimizing the error function, i.e.,

$$\text{find } \hat{\boldsymbol{\theta}} = \arg\min_{\boldsymbol{\theta}} \; L_n(Y;\boldsymbol{\theta}) \tag{2.22}$$

Since there are four parameters in the vector $\boldsymbol{\theta}$, a sequence of optimization steps are taken. We start by taking partial derivative of the error function with respect to the unknown phase ϕ_A, which yields

$$\frac{\partial L_n(Y;\boldsymbol{\theta})}{\partial \phi_A} = 2b \sum_{m=0}^{M-1}\sum_{n=0}^{N-1} \Big(2\Re\big\{ -jY_{m,n} be^{-j\phi_A} e^{-j2\pi(m f_d T_s Q N - n\Delta f \tau)} \big\} \Big) = 0 \tag{2.23}$$

Note that the 2-D discrete time Fourier transform of $Y_{m,n}$ is

$$Z(f_d, \tau) = \sum_{m=0}^{M-1} \Big(\sum_{n=0}^{N-1} Y_{m,n} e^{j2\pi n \Delta f \tau} \Big) e^{-j2\pi m f_d T_s Q N} \tag{2.24}$$

Inserting (2.24) in (2.23) we obtain

$$\Re\big\{ -jbe^{-j\phi_A} Z(f_d, \tau) \big\} = 0 \tag{2.25}$$

Since b and $|Z(f_d,\tau)|$ are positive real values, only the real component of the phase term must be zero. Hence we have

$$\cos\Big(\frac{\pi}{2}+\phi_A-\angle Z(f_d,\tau)\Big)=0 \tag{2.26}$$

This is a simple trigonometric equation and the solution is

$$\hat{\phi}_A=k\pi+\angle Z(f_d,\tau), \tag{2.27}$$

where k is an integer. Using this estimate (2.27) in the error function (2.21) and ignoring the terms independent of b, we obtain

$$L_n(Y;\hat{\phi}_A,b,f_d,\tau)=2b\Re\big\{e^{-\angle Z(f_d,\tau)}Z(f_d,\tau)\big\}-MNb^2 \tag{2.28}$$

which simplifies to

$$L_n(Y;\hat{\phi}_A,b,f_d,\tau)=2b|Z(f_d,\tau)|-MNb^2 \tag{2.29}$$

By equating the partial derivative with respect to b to zero yields

$$\hat{b}=\frac{|Z(f_d,\tau)|}{MN} \tag{2.30}$$

Inserting the estimate (2.30) in (2.29) we obtain

$$L_n(Y;\hat{\phi}_A,\hat{b},f_d,\tau)=\frac{|Z(f_d,\tau)|^2}{MN} \tag{2.31}$$

which is a scaled the periodogram of the 2D-DTFT in (2.24). Hence, we obtain the final optimization problem for unknown delay and doppler frequency parameters as

$$\text{find}\ \ \hat{f}_d,\hat{\tau}=\arg\max_{f_d,\tau}\frac{|Z(f_d,\tau)|^2}{MN} \tag{2.32}$$

The solution to (2.32) can be determined by finding the peak of un-windowed 2D periodogram of the signal $Y_{m,n}$. This estimation can be accomplished by a two-dimensional search [Rife and Boorstyn, 1974].

2.4 Cramer-Rao Lower Bounds

Note that if $W_{m,n}$ in (2.18) is a Gaussian random process, $\hat{\boldsymbol{\theta}}$ is a large sample realization of the maximum-likelihood estimator of $\boldsymbol{\theta}$. Since the maximum-likelihood estimator is expected to achieve the Cramer-Rao Low Bound (CRLB) as M or N increases, it follows that under the Gaussian assumption no other estimator could perform better in large samples than $\hat{\boldsymbol{\theta}}$. In this section, we derive the Cramer-Rao lower bound of $\hat{\boldsymbol{\theta}}$. The probability model of the measurements $Y=\{Y_{m,n}\}$ is

$$P(Y|\boldsymbol{\theta})=\prod_{m=0}^{M-1}\prod_{n=0}^{N-1}\frac{|a_{m,n}|^2}{\pi\sigma_w^2}\exp\left(-\frac{|a_{m,n}|^2}{\sigma_w^2}|Y_{m,n}-be^{j\phi_A}e^{j2\pi(mf_dT_sQN-n\Delta f\tau)|^2}|^2\right) \tag{2.33}$$

The log-likelihood function is

$$l(Y|\boldsymbol{\theta})=-\sum_{m=0}^{M-1}\sum_{n=0}^{N-1}\Big(|Y'_{m,n}|^2+b^2|a_{m,n}|^2-2\Re\{Y^*_{m,n}be^{j\phi_A}a_{m,n}e^{j2\pi(mf_dT_sQN-n\Delta f\tau)}\}\Big) \tag{2.34}$$

The Cramer-Rao bounds for the parameter estimates $\hat{\theta}_i$ are given by the diagonal elements of inverse of the 4×4 Fisher information matrix $\mathbf{J}$ [Kay, 1993],

$$\mathrm{Var}(\hat{\theta}_i) \geq [\mathbf{J}^{-1}]_{ii} \tag{2.35}$$

where θ_i are the four scalar parameters in the vector $\boldsymbol{\theta}$ in (2.19) with $i = 1, 2, 3, 4$.

Due to space limitations, a detailed derivation of the elements are omitted in this work. We only present the final results here. The determinant of Fisher information matrix $\mathbf{J}$ is

$$\det(\mathbf{J}) = \frac{256b^6}{\sigma_w^8}(Ma\pi^2 T_s Q N \Delta f)^2 (MQ_M - P_M^2)(aQ_N - P_N^2) \tag{2.36}$$

where $P_M = \sum_{m=0}^{M-1} m = M(M-1)/2$, $Q_M = \sum_{m=0}^{M-1} m^2 = M(M-1)(2M-1)/6$, $Q_N = \sum_{n=0}^{N-1} n^2 |a_{m,n}|^2$ and $P_N = \sum_{n=0}^{N-1} n|a_{m,n}|^2$. The Cramer-Rao low bound on the estimate of b is the first element along the diagonal of $\mathbf{J}^{-1}$ given by

$$\mathrm{CRB}_b = \frac{1}{\det(\mathbf{J})}(MQ_M - P_M^2)(Q_N - P_N^2)\frac{128b^6}{\sigma_w^6} \\ Ma\pi^4 (T_s Q N)^2 (\Delta f)^2 \tag{2.37}$$

The diagonal elements of the $\mathbf{J}^{-1}$ are evaluated using the adjoint method. Next, using (2.36) and upon simplification we obtain $\mathrm{CRB}_b = \frac{\sigma_w^2}{2Ma}$. The CRLB on ϕ_A is the second element along the diagonal of $\mathbf{J}^{-1}$ and is obtained as,

$$\mathrm{CRB}_{\phi_A} = \frac{\sigma_w^2}{b^2}\frac{MaQ_M Q_N - P_M^2 P_N^2}{2Ma(MQ_M - P_M^2)(aQ_N - P_N^2)} \tag{2.38}$$

The CRLB on f_d is the third element along the diagonal of $\mathbf{J}^{-1}$ given by,

$$\mathrm{CRB}_{f_d} = \frac{1}{\det(\mathbf{J})}\frac{8b^6}{\sigma_w^6}\frac{M^3 a}{b^2}(2\pi\Delta f)^2 (aQ_N - P_N^2) \tag{2.39}$$

Again upon simplification we obtain

$$\mathrm{CRB}_{f_d} = \frac{M\sigma_w^2}{8ab^2\pi^2 (T_s Q N)^2 (MQ_M - P_M^2)} \tag{2.40}$$

Finally, the CRLB on τ is the forth element along the diagonal of $\mathbf{J}^{-1}$ defined as,

$$\mathrm{CRB}_\tau = \frac{1}{\det(\mathbf{J})}\frac{8b^6}{\sigma_w^6}\frac{Ma^3}{b^2}4\pi^2 (T_s Q N)^2 (MQ_M - P_M^2) \tag{2.41}$$

Hence, upon simplification we obtain

$$\mathrm{CRB}_\tau = \frac{a\sigma^2}{2(aQ_N - P_N^2)b^2 M(2\pi\Delta f)^2} \tag{2.42}$$

2.5 Weighted OFDM Symbol Design

We use the classic Cramer-Rao lower bound (CRLB) to evaluate the performance of the nonlinear least-squares estimation. Eqn. (2.42) reveals that the CRLB on time delay estimate $\hat{\tau}$ is determined by the factor $\frac{\sigma_w^2}{b^2}$, a term related to SNR, the number of pulses M, the frequency separation Δf and the factor $\frac{a}{aQ_N - P_N^2}$ which depends on OFDM symbol amplitudes $|a_{m,n}|$. Similarly, Eqn. (2.40) shows that CRLB on the Doppler frequency estimate $\hat{f}_d$ depends on the SNR value $\frac{ab^2}{\sigma_w^2}$, the constant $\frac{M}{MQ_M - P_M^2}$ and the sampled length of the pulse repetition interval $T_s QN$, but independent of the spectral shape of OFDM symbols $|a_{m,n}|$.

By the definition of CRLB, we know that the determinant of the Fisher information matrix $\det(\mathbf{J})$ in (2.36) is the common denominator for each of the CRLBs given in (2.37), (2.38), (2.40) and (2.42). The aim for weighted OFDM is to design OFDM symbols to minimize the inverse of $\det(\mathbf{J})$ subject to proper constraints, i.e.,

$$\text{find } a_{m,n} \quad = \quad \arg\min_{a_{m,n}} \frac{1}{aQ_N - P_N^2} \tag{2.43}$$

$$\text{s.t} \quad \begin{cases} \text{(C1)} & \min(|a_{m,n}|) > \eta_0 \max(|a_{m,n}|) \\ \text{(C2)} & \text{PAPR} < \eta_1 \\ \text{(C3)} & \sum_{n=0}^{N-1} |a_{m,n}|^2 \le a \end{cases} \tag{2.44}$$

Condition (C1) is to impose a constraint on the lower bound of the cost function $\frac{1}{aQ_N - P_N^2}$ by

$$\frac{\min(|a_{m,n}|)}{\max(|a_{m,n}|)} < \eta_0 \le 1 \tag{2.45}$$

The purpose of this constraint is to avoid bandwidth loss. Otherwise, OFDM symbols $a_{m,n}$ would allocate zero power in most of sub-bands n, causing bandwidth loss in the transmission signal. As a result, the range resolution could be severely degraded. Condition (C2) is to set an upper bound $\eta_1 \ll N$ on the peak to average power ratio (PAPR) defined by

$$\text{PAPR} = a^{-1} \max_{0<t<T_p} |s_m(t)|^2 \tag{2.46}$$

because a high PAPR imposes severe burden on the transmitter due to limited amplification range of the RF amplifier. For instance, when phase shift keying (PSK) is used, the upper bound on PAPR is N [Ochiai and Imai, 2001]. Finally, Condition (C3) is the total power constraint. The optimization problem defined in (2.43) and (2.44) is solved numerically using convex optimization by the active-set constrained nonlinear method [Han, 1977].

2.6 Simulation Results

The estimation performance of the proposed weighted OFDM (WOFDM) is compared with the QPSK based constant envelope OFDM (CE-OFDM) scheme. For QPSK, we choose $|a_{m,n}|^2 = 1/N$. The phase of the OFDM symbols $a_{m,n}$ is a uniformly distributed random variable. Under this modulation scheme, the cost function $aQ_N - P_N^2 = \frac{N^2-1}{12}$ is a constant. The CRLB of the Doppler in (2.40) is independent of modulation. The CRLB of delay estimate for CE-OFDM is also independent of symbol amplitude $|a_{m,n}|$ and is given by

$$CRB_\tau = 3\sigma^2 / \left(2(N^2-1)b^2 M(\pi \Delta f)^2\right) \tag{2.47}$$

For WOFDM, both amplitude and phase of the weights $a_{m,n}$ are derived from the optimization problem (2.43) and (2.44). In the simulations, the bandwidth $B = 10$ MHz, the number of subcarriers is $N = 128$, and the carrier frequency is $f_c = 2$ GHz. The frequency separation is $\Delta f = 781.25$ kHz. The signal energy is normalized (i.e., $a = 1$) and the SNR varies from $1 \sim 13$ dB. The pulse repetition interval is $T_{PRI} = NT_p$. The resolution of the Doppler spectrum is $1/(T_s QNM)$. The delay spectrum has a resolution of $T_{PRI}/N = T_p$.

The true values of parameters of a simulated moving target are given as follows. The Doppler frequency is $f_d = .5/T_{PRI}$, time delay is $\tau = T_{PRI}/2$ and the number of pulses is $M = 50$. The optimization parameters are set as $\eta_0 = 0.2$ and $\eta_1 = 3$. The estimates $\hat{f}_d$ and $\hat{\tau}$ are obtained by the nonlinear least-squares estimator formulation in (2.32). By the active-set constraint optimization method, we calculate the weights $a_{m,n}$ numerically [Han, 1977]. Table 2.1 presents the statistics of

Table 2.1: Variations of PAPR Values

Modulation	CE-OFDM	WOFDM
average PAPR	5.643	3.004
variance	1.348	0.016

PAPR from the CE-OFDM vs. WOFDM. The WOFDM method yields a more stable (i.e., smaller variance) and lower PAPR value compared to the CE-OFDM method.

Fig. 3.1 depicts the theoretical CRLB and the numerical values for the delay and Doppler estimates. For the delay estimate in Fig. 3.1(a), the plots show that WOFDM modulation given in (2.42) achieves a smaller CRLB than CE-OFDM given in (2.47). This is because by varying the magnitudes of the OFDM symbols, we reduce the value of the $\max(|s_m(t)|)$, i.e., bringing it closer to the mean value of $(|s_m(t)|)$. Hence we achieve a higher value for $\det(\mathbf{J})$, thus leading to a lower CRLB for delay estimate. As expected, for Doppler estimate, the CRLBs are the same for the two modulation schemes. Note that the variance plots of the parameter estimates by the WOFDM method closely follows the variance plots of CE-OFDM only after the SNR goes above 8 dB. This phenomenon is often called threshold effect in nonlinear estimation problem [Rife and Boorstyn, 1974]. It means at low SNR, there is usually a range of SNR in which the mean-squared error (MSE) rises rapidly as SNR decreases. In other words, only at high SNR, the computed SNR follow the CRLB closely, as shown in Fig. 3.1. Fig. 3.2 represents the improvements in CRLB using the WOFDM compared to the CE-OFDM with respect to different values of η_0 and η_1. The plots show the tradeoff between the CRB, PAPR and bandwidth preservation, i.e., it is not possible to achieve low CRB and low PAPR simultaneously.

2.7 Conclusion

A weighted OFDM scheme is proposed which provides a lower PAPR compared to the QPSK based constant envelope OFDM scheme. Theoretical analysis and numerical simulation demonstrate that the CRLB bound for Doppler (velocity) estimate does not change with modulation, however, the CRLB of delay (range) estimate is improved with the weighted symbols by WOFDM. The proposed WOFDM scheme provides a promising means to achieve co-existence between radar and communications via a reconfigurable RF platform.

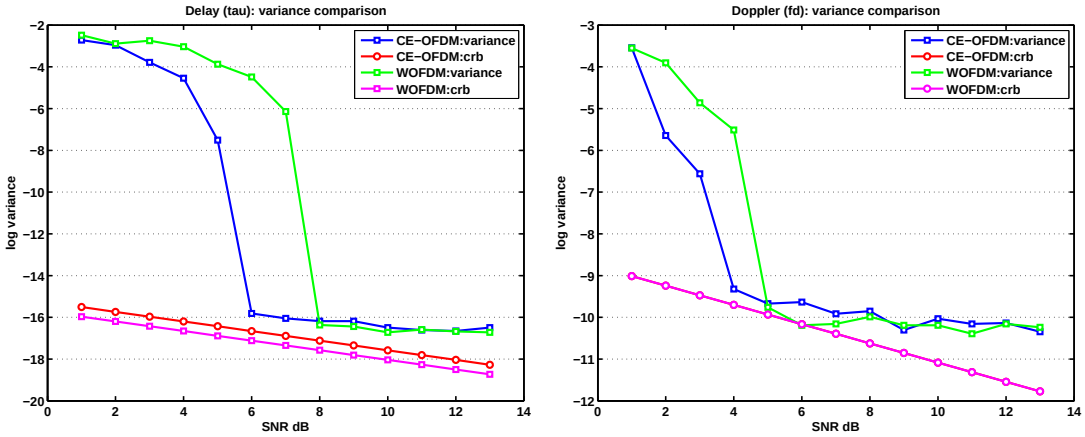

(a) (b)

Figure 2.1: Computed variance and CRLB for CE-OFDM vs. WOFDM modulation. (a) Delay estimate $\hat{\tau}$. (b) Doppler frequency estimate $\hat{f}_d$

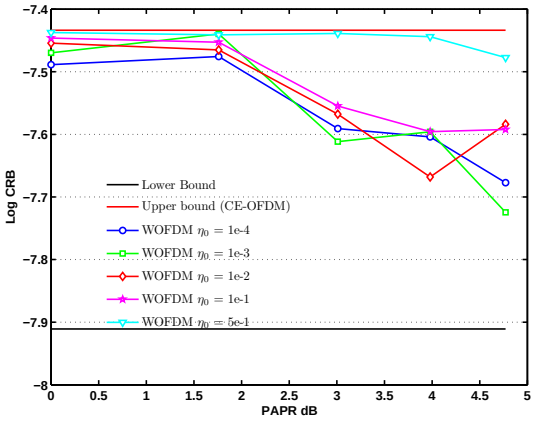

Figure 2.2: CRLB for WOFDM, a compromise between the upper bound (CE-OFDM), lower bound and PAPR

Chapter 3

Waveform Encoding for Nonlinear Electromagnetic Tomographic Imaging

3.1 Introduction

Electromagnetic (EM) tomographic imaging is an inverse scattering problem which has a wide range of applications in medical imaging, geophysical exploration, nondestructive testing, and target identifications [Chew and Wang, 1990, Franchois and Pichot, 1997, Isernia et al., 1997]. In EM tomographic imaging, source antennas transmit EM signals into a medium under test and receive scattering signals. Based on the underlying Maxwell's equations, inversion methods are employed to reconstruct a spatial distribution of material parameters such as the dielectric permittivity and/or magnetic permeability of the target and the surrounding medium, thus turning recorded scattering data into images [Fhager et al., 2006, Liu et al., 2002].

Mathematically, electromagnetic tomographic imaging is an inverse problem, which can be written as

$$y_j = \mathcal{A}_j(p(\mathbf{r}); s_j) + \eta_j,\ j = 1, \cdots, Q \tag{3.1}$$

The goal is to infer model parameters (i.e., material property values $p(\mathbf{r}), \mathbf{r} \in \Omega$) from the observed data (i.e., measurement $y_j \in \partial\Omega \times [0, T]$) in response to the j-th excitation source s_j based upon a Maxwell wave model. Ω denotes the imaging field, T is the integration time of the signals measured at the receivers positioned at the boundary $\partial\Omega$ of the imaging field. Q is the number of excitation sources. $\mathcal{A}_j(\cdot)$ is the nonlinear operator determined by the wave model and η_j is the noise or disturbance term. The image to be reconstructed is a spatial distribution of the parameter p. The dimension of p, determined by the discretization of the image field Ω, is often much larger than the dimension $|\partial\Omega|$ (i.e., the number of receivers) for data y_j. Hence, the full-wave inverse problem (3.1) is considered ill-posed, often requiring regularization of the inverse problem. For example, the well known compressive sensing method would impose a sparsity constraint on p [Candes and Tao, 2006, Lustig et al., 2008], thus effectively reducing the dimensionality of the solution space for p.

The imaging problem (3.1) we consider is more challenging in that it involves solving a nonlinear full wave inverse problem with active excitation sources. Classic approaches to solving (3.1) include the least squares optimization method [He et al., 1997, Jia et al., 2002] or the iterative Newton's method [Dorn et al., 1999]. In both cases, iterative computational techniques are employed.

The cost of computation depends on the size of the data volumes (i.e., the number of transmission sources and the number of receivers) and on the discretization of the wave model. The complexity of computing gradient and Newton updates - aside from issues with non-convergence and

non-uniqueness - become the major impediment withstanding successful application of full wave inversion to industry-size data volumes, for example, large scale seismic imaging [Krebs et al., 2009] and high resolution medical imaging [Fhager et al., 2006].

In this work, we will address this issue by means of dimensionality reduction through multiple source waveform encoding. Typical full wave tomographic imaging operates in a single-input multiple-output (SIMO) configuration. An image is reconstructed from measured data in response to a single excitation antenna source. The reconstruction process continues till all the sources are excited. For large-scale imaging such as seismic exploration, the number of EM sources is very large. Not only the computational cost is high, the operational expenditures of each data collection process is also significant. In this case, multiple source excitation becomes appealing. For example, in seismic imaging, multiple sources are excited simultaneously to form a so-called supershot to probe the imaging field [Godwin and Sava,], which means the imaging configuration becomes multiple-input multiple-output (MIMO).

The recorded data are processed to form an image. The image is updated when new measurement data is available. This procedure is repeated until the image converges or a pre-determined stopping criterion is met. However, multiple wave simultaneous excitation induces cross-talk noise due to wave interference, which, if not treated, will cause image artifacts. Therefore, signal processing techniques such as waveform encoding are needed to mitigate cross-talk noise in the image in order to achieve high quality imaging while reducing the computational complexity.

The contribution of this work is threefold. First, we develop three different waveform encoding techniques, i.e., random phase encoding, waveform delay encoding, and uniform weight encoding for the full-wave EM imaging problem. We show that the random phase encoding method results in constant-envelop waveforms and produces the best performance in terms of convergence. Second, this work extends our early work on microwave imaging in a SIMO configuration [Dong et al., 2012]. We show that using simultaneous sources made of superposition of encoded sources is able to accelerate iterative algorithms for electromagnetic full-wave inversion, thus demonstrating the effectiveness of waveform encoding, a common signal processing technique, to improve computational efficiency of classic nonlinear inverse problems. Third, although waveform encoding techniques have been studied for acoustical wave imaging [Krebs et al., 2009] and our early work on MIMO ultrasonic imaging [Dong and Jin, 2013, Dong et al., 2014], there is still a lack of research for EM full-wave imaging in applications where the use of EM wave energy is critical. In this work, we develop iterative algorithms that solve time domain Maxwell's equations with coupled electric fields and magnetic fields using waveform encoded excitations and demonstrate faster convergence compared with our prior SIMO imaging algorithm in [Dong et al., 2012].

3.2 MIMO Imaging Problem Formulation

Consider the time dependent Maxwell's equations in an isotropic medium [Chew, 1994]

$$\epsilon(\mathbf{r})\frac{\partial \vec{E}(\mathbf{r},t)}{\partial t} - \nabla \times \vec{H}(\mathbf{r},t) + \sigma(\mathbf{r})\vec{E}(\mathbf{r},t) = -\vec{J}(\mathbf{r},t) \tag{3.2}$$

$$\mu(\mathbf{r})\ \frac{\partial \vec{H}(\mathbf{r},t)}{\partial t} + \nabla \times \vec{E}(\mathbf{r},t) = 0 \tag{3.3}$$

where the quantities $\vec{E}(\mathbf{r},t) = (E_x, E_y, E_z, t)$ and $\vec{H}(\mathbf{r},t) = (H_x, H_y, H_z, t)$ are the electric and magnetic field intensities defined on $\Omega \times [0,T]$, where $\mathbf{r} \in \Omega$ is the imaging region. The material parameters including electrical permittivity $\epsilon(\mathbf{r})$, magnetic permeability $\mu(\mathbf{r})$ and conductivity $\sigma(\mathbf{r})$ are independent of time. The quantity $\vec{J}(\mathbf{r},t) = (J_x, J_y, J_z, t)$ is the electric current density of an

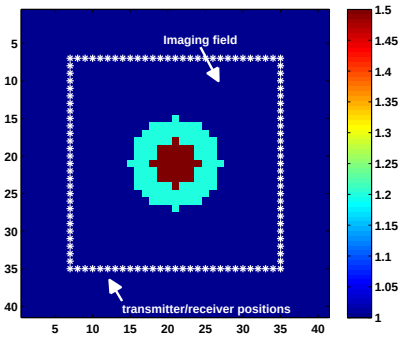

Figure 3.1: 2D MIMO tomographic imaging geometry. At the m-th transmission, the m-th group of multiple current sources are excited to emit TM waves to interrogate the imaging field. Scattered signals are received by all the sensors.

external charge and is considered as the external source. The initial conditions are $\vec{E}(\mathbf{r}, 0) = 0$ and $\vec{H}(\mathbf{r}, 0) = 0$.

3.2.1 2D EM tomographic imaging problem

We consider a 2-D inverse scattering problem where only the transverse magnetic (TM) waves are studied. In this case, $E_z \neq 0, H_z = 0$. Furthermore, for the sake of simplicity, we assume that only the E_z component is recorded, i.e., we let $E_x = E_y = 0$. By omitting the space parameter $\mathbf{r}$ for the moment, the Maxwell's equations in (3.2) and (3.3) become

$$\frac{\partial E_z}{\partial t}(t) = -\frac{\sigma}{\epsilon} E_z(t) + \frac{1}{\epsilon}\left(\frac{\partial H_y}{\partial x} + \frac{\partial H_x}{\partial y}\right)(t) - \frac{1}{\epsilon} J_z(t) \tag{3.4}$$

$$\frac{\partial H_y}{\partial t}(t) = \frac{1}{\mu}\frac{\partial E_z}{\partial x}(t), \quad \text{and} \quad \frac{\partial H_x}{\partial t}(t) = -\frac{1}{\mu}\frac{\partial E_z}{\partial y}(t) \tag{3.5}$$

where $J_z(t)$ is the current source polarized in the z-direction emitted from the transmit antennas. Specifically, in the tomographic imaging setup shown in Fig. 3.1, the excitation signal source can be expressed by

$$J_{z,j}(\mathbf{r}, t) = s_j(t)\delta(\mathbf{r} - \mathbf{r}_j^t), \quad j = 1, 2, \cdots, Q \tag{3.6}$$

where $\mathbf{r}_j^t$ is the position of the j-th transmit antenna. Q is the total number of transmitters. $s_j(t)$ is the excitation signal emitted by the j-th transmitter. $\delta(\mathbf{r})$ is the Dirac delta function. The short pulsed signal generated by a source illuminates the imaging field and the unknown target. The transient field data are collected at the receiver positions $\mathbf{r}_j^r$. Furthermore, we assume in this work that the transmitter and the receiver positions are the same, i.e., $\mathbf{r}_j^r = \mathbf{r}_j^t$.

Next we combine L_m individual excitation sources at the m-th transmission, leading to the m-th "supershot"

$$J_{z,m}(\mathbf{r}^t, t) = \sum_{j=1}^{L_m} J_{z,j}(\mathbf{r}_j^t, t), \ m = 1, \cdots M \tag{3.7}$$

which is the combined $L_m \geq 1$ sources. Note that the total number of sources remains unchanged, i.e., $Q = \sum_{m=1}^{M} L_m$. When $L_m = L$ is a constant, then $M = Q/L$. It is easy to see when $L_m = 1$, the MIMO configuration reduces to the SIMO configuration.

Next, let the symbol $p = [\epsilon \ \ \sigma \ \ \mu]^T$ denote the parameter vector which stands for the material properties of the internal structure of the medium (or objects) to be reconstructed. The imaging problem is to seek the solution of the nonlinear equations

$$\tilde{E}_{z,m}(\mathbf{r}_j^r, t) = E_{z,m}(p; \mathbf{r}_j^r, t) + \eta_m \tag{3.8}$$

where $m = 1, \cdots, M$ is the index for transmission sources and $j = 1, \cdots, Q$ is the index for receivers. $\tilde{E}_{z,m}(\mathbf{r}_j^r, t)$ is the measured z-component of the electric field at the receiver antenna position $\mathbf{r}_j^r$. $E_{z,m}(p; \mathbf{r}_j^r, t)$ is the calculated electric field for the parameter p at the j-th receiver position $\mathbf{r}_j^r$ in response to the m-th excitation source $J_{z,m}(\mathbf{r}^t, t)$. The calculation of $E_{z,m}(p; \mathbf{r}_j^r, t)$ is based upon the underlying Maxwell's equations (3.4) and (3.5). Next, organizing all the measured electrical field data into a space-time matrix with respect to $(\mathbf{r}^r, t)$

$$\tilde{\mathbf{e}}_m = [\tilde{E}_{z,m}(\mathbf{r}_1^r, t), \tilde{E}_{z,m}(\mathbf{r}_2^r, t), \cdots, \tilde{E}_{z,m}(\mathbf{r}_Q^r, t)]^T \tag{3.9}$$

Accordingly, the imaging problem (3.8) can be written as a system of nonlinear operator equations

$$\tilde{\mathbf{e}}_m = \boldsymbol{\mathcal{A}}_m(p; J_{z,m}(\mathbf{r}^t, t)) + \boldsymbol{\eta}_m \tag{3.10}$$

where the j-th component $[\boldsymbol{\mathcal{A}}_m(p; J_{z,m}(\mathbf{r}^t, t))]_j \triangleq E_{z,m}(p; \mathbf{r}_j^r, t)$ is the calculated electrical field at the j-th receiver antenna. $\boldsymbol{\eta}_m$ is the additive noise or disturbance. The problem of interest is to find out the solution $p(\mathbf{r})$ for (3.10) over the imaging region $\mathbf{r} \in \Omega$ given proper initial condition and boundary conditions and waveform encoded excitation signals $J_{z,m}(\mathbf{r}^t, t)$.

3.2.2 Inversion algorithm by adjoint fields

We use iterative Newton's method to calculate the material property value p. Let $p^{(0)}$ be the initial approximation, the update equation is given by

$$p^{k+1} = p^k + \gamma \delta p^k \tag{3.11}$$

where γ is a relaxation factor. δp^k is the increment value at k-th iteration. We employ the adjoint method to calculate δp^k [Dong et al., 2012], which takes the form of

$$\delta p^k = \left(\boldsymbol{\mathcal{A}}'_m(p^k, J_{z,m}(\mathbf{r}^t, t))\right)^* \mathbf{d}^k, \ m = k \mod M \tag{3.12}$$

where $\mathbf{d}^{(k)} \triangleq \tilde{\boldsymbol{e}}_m - \boldsymbol{e}_m^{(k)}|_{\partial\Omega\times[0,T]}$ is the difference signal. $\boldsymbol{e}_m^{(k)}|_{\partial\Omega\times[0,T]} = \boldsymbol{\mathcal{A}}_m(p^{(k)}, J_{z,m}(\mathbf{r}^t, t))$ is the calculated electric field signal value at the boundary at the k-th iteration in response to the m-th transmission. Here the symbol $\boldsymbol{\mathcal{A}}'_m(\cdot)$ stands for a locally uniformly bounded Fréchet derivative of $\boldsymbol{\mathcal{A}}_m(\cdot)$ and $\boldsymbol{\mathcal{A}}'_m(\cdot)^*$ is the adjoint operator of $\boldsymbol{\mathcal{A}}'_m(\cdot)$ [Dorn et al., 1999, Dong and Jin, 2013]. The symbol $\mod$ stands for the modulo operation.

The outline of the algorithm is given in Table 3.1. The inversion algorithm involves four steps. Step 1 solves a forward problem, i.e., from k-th value p^k, we calculate the projected value $\boldsymbol{\mathcal{A}}_m(p^k; J_{z,m}(\mathbf{r}^t, t))$ at the boundary of the imaging field $\partial\Omega$, which yields $\boldsymbol{e}_m^k$. Step 2 calculates the difference signal $\mathbf{d}^k$. Step 3 is the inversion algorithm that calculates the adjoint fields $\left(\boldsymbol{\mathcal{A}}'_m(p^k; J_{z,m}(\mathbf{r}^t, t))\right)^*$. Step 4 computes the update and evaluates the stopping criterion. From the operator point of view, we can show from (3.7) that $\boldsymbol{\mathcal{A}}_m(p; J_{z,m}(\mathbf{r}^t, t)) = \sum_{j=1}^{L_m} \boldsymbol{\mathcal{A}}_j(p; J_{z,j}(\mathbf{r}_j^t, t))$. We omit the proof due to space limitations.

Table 3.1: Full Wave Inversion Algorithm by Adjoint Fields

Initialize	$p \leftarrow p^0$	
Iteration	**while** $\|p^{k+1} - p^k\|^2 \geq \epsilon$ **do**	
	1. $\boldsymbol{e}_m^k = \boldsymbol{\mathcal{A}}_m(p^k)$	// forward problem
	2. $\mathbf{d}^k \triangleq \tilde{\boldsymbol{e}}_m - \boldsymbol{e}_m^k$	// difference signal
	3. $\delta p^k = \left(\boldsymbol{\mathcal{A}}'_m(p^k)\right)^* \ \mathbf{d}^k$	// adjoint fields
	4. $p^{k+1} = p^k + \gamma \delta p^k$	// update
	end	

3.3 Waveform Encoding in EM Imaging

MIMO waveform signaling is well studied in signal processing community to improve spatial diversity for better estimation and detection [Jin et al., 2010]. In this work, the goal of MIMO signaling is to improve computational efficiency of nonlinear imaging by accelerating the convergence of the iterative algorithm while achieving high resolution images. We consider a Gaussian modulated pulse as the basic excitation signal, which takes the form of $s_j(t) = s(t) = \cos(2\pi f_c t) e^{-2\pi^2 t^2/\tau_p^2}$ where τ_p is the pulse width. Next, we examine three waveform encoding techniques for imaging.

3.3.1 Waveform encoding design

(1) Random phase encoding. The method applies a random phase term $w_j = e^{i\theta_j}$ to each excitation signal $s_j(t)$, where i denotes the imaginary unit and $\theta_j = \text{Uniform}(0, 2\pi)$. In particular, we consider binary phase shift keying scheme where only $\{e^{i\pi} = -1\}$ and $\{e^{i0} = +1\}$ are chosen randomly following a Bernoulli distribution. Hence, the aggregated excitation signal takes the form of

$$J_{z,m}^{(1)}(\mathbf{r}^t, t) = \sum_{j=1}^{L_m} w_j s_j(t) \delta(\mathbf{r}^t - \mathbf{r}_j^t), \ m = 1, \cdots M \tag{3.13}$$

Our simulation studies reveal that this method reduces cross-talks while achieving accelerated convergence.

(2) Time-delays encoding. To reduce the cross-talks, a fixed time delay τ_j is applied to the L_m sources at the m-th transmission.

$$J_{z,m}^{(2)}(\mathbf{r}^t, t) = \sum_{j=1}^{L_m} s_j(t - \tau_j) \delta(\mathbf{r}^t - \mathbf{r}_j^t), \ m = 1, \cdots M \tag{3.14}$$

where τ_j is the relative delay for the j-th source. A good choice of time delay is the pulse width, i.e., $\tau_j = \tau_p$, for Gaussian modulated pulses.

(3) Uniform weight encoding. In this case, $L_m > 1$ excitation signals are emitted simultaneously from L_m antennas, the aggregated electric current density becomes

$$J_{z,m}^{(1)}(\mathbf{r}^t, t) = \sum_{j=1}^{L_m} s_j(t) \delta(\mathbf{r}^t - \mathbf{r}_j^t), \ m = 1, \cdots M \tag{3.15}$$

However, the mutual interference between the excitation signals may cause cross-talks, which degrades the image quality.

3.3.2 Impact of excitation sources

To examine the impact of the excitation sources on the solution of the imaging problem, we re-write the Maxwell's equation as a second order wave equation. Starting from the Farday's Law in the vector form, $\nabla \times \vec{E} = -\mu \frac{\partial \vec{H}}{\partial t}$, and take the curl of both sides, we obtain $\nabla \times \nabla \times \vec{E} = -\mu \frac{\partial}{\partial t}(\nabla \times \vec{H})$. Note that $\nabla \times \nabla \times \vec{E} = -\nabla^2 \vec{E}$, and using (3.2), we obtain

$$\nabla^2 \vec{E} = \mu\epsilon \frac{\partial^2 \vec{E}}{\partial t^2} + \mu \frac{\partial}{\partial t}\left(\vec{J} + \sigma \vec{E}\right) \tag{3.16}$$

Next, consider the TM mode where only E_z is to be reconstructed, we can re-write (3.16) as a second-order scalar wave equation

$$\frac{\partial^2 E_z}{\partial t^2} - c^2 \frac{\partial^2 E_z}{\partial z^2} = f(z,t) \tag{3.17}$$

where the forcing term in (3.17), $f(z,t) = \frac{1}{\epsilon}\frac{\partial}{\partial t}(J_z + \sigma E_z)$, depends on the excitation source J_z. More importantly, by the theory of wave equation [Evans, 2010], the solution to inhomogeneous wave equation (3.17) can be written as, $E_z = E_{z,g} + E_{z,p}$, the sum of the general solution $E_{z,g}$ of the homogeneous wave equation (i.e., (3.17) when setting $f(z,t) = 0$) and the particular solution $E_{z,p}$, [Evans, 2010], where

$$E_{z,p} = \frac{\sqrt{\mu\epsilon}}{2} \int_0^t \int_{z-(t-t')/\sqrt{\mu\epsilon}}^{z+(t-t')/\sqrt{\mu\epsilon}} f(z,t) dz dt \tag{3.18}$$

Eqn. (3.18) reveals that the electric field computed in the forward model depends on the excitation source, which also affects the reconstruction procedure for tomographic imaging. However, an exact relationship between the excitation sources J_z and the quality of imaging $\epsilon(\mathbf{r})$ by iterative algorithm (i.e., convergence speed and reconstruction error) is implicit. Here we rely on numerical means to study how source encoding schemes effect the quality of tomographic imaging.

3.4 Numerical Experiments

In this section, we conduct numerical experiments to test and verify our results. The test example is shown in Fig. 3.1. The object to be reconstructed is a two-layer dish-like objects. The inner object is of diameter of 6 mm with a dielectric constant $\epsilon = 1.2\epsilon_0$ and the outer object is of diameter of 12 mm with a dielectric constant $\epsilon = 1.5\epsilon_0$. ϵ_0 is the vacuum permittivity $8.85 \times 10^{-12}\, F/m$. The permittivity value for the surrounding medium is ϵ_0. In the simulation, only the permittivity $\epsilon(\mathbf{r})$ is to be reconstructed. The conductivity value is set to zero $\sigma = 0$, and the magnetic permeability is chosen to be a constant $\mu = \mu_0 = 4\pi \times 10^7 H/m$. The antennas are placed on the four sides of the imaging region. There are a total of 90 co-located transmitters/receivers. The computational area is a square region having sides of length 12 cm and is discretized to 40 by 40 grids. In the computation, we use the MUR absorbing boundary condition [Mur, 1981]. 5% of random disturbance as $\boldsymbol{\eta}_m$ is introduced to the simulated electric wavefield signals. To evaluate the performance of the iterative algorithms with different encoding schemes, we calculate the relative error

$$\beta = \|\hat{\epsilon}^{(k)} - \epsilon_{\text{true}}\|^2 / \|\hat{\epsilon}^{(0)} - \epsilon_{\text{true}}\|^2 \tag{3.19}$$

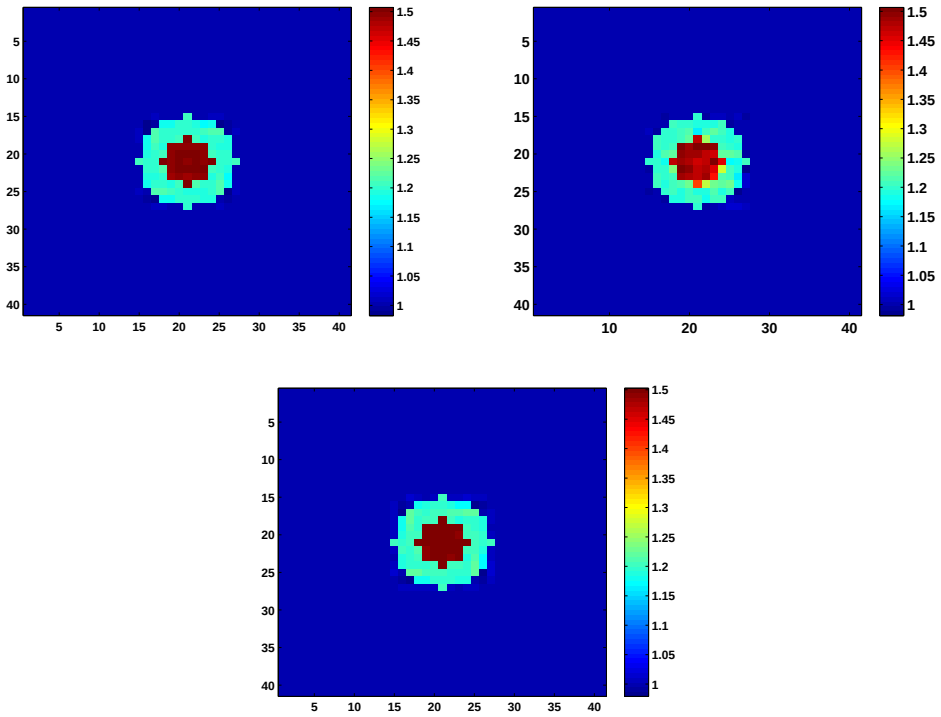

Figure 3.2: Reconstructed images of dielectric value ϵ. Top: random phase encoding. Middle: waveform delay encoding. Bottom: uniform weight encoding.

where $\hat{\epsilon}^{(0)}$ and $\hat{\epsilon}^{(k)}$ is the initial and final value of the reconstructed image, respectively. ϵ_{true} is the true value of the dielectric constant of the target and the medium.

Simulations are conducted using $L_m = 7$ excitation sources at each transmission under the three different waveform encoding schemes. Fig. 3.2 depicts three reconstructed images under the random phase encoding (3.13), waveform delay encoding (3.14), and uniform encoding (3.15). Fig. 3.3 depicts the corresponding convergence history (i.e., relative residual error β vs. the CPU run time in seconds) of the three iterative algorithms. The conventional single source excitation scheme is also included. Among the three encoding schemes, the random phase encoding achieves fastest convergence and smallest imaging error, compared with the uniform waveform encoding and the waveform delay encoding schemes. As expected, the conventional SIMO imaging yields the slowest convergence and lowest image quality at the 450 seconds compared with other three encoding techniques, as shown in Fig. 3.3.

3.5 Conclusions and Discussions

We developed waveform encoding techniques for a nonlinear electromagnetic tomographic imaging problem in the time domain. Proper encoding techniques such as random phase encoding yields fast convergence of iterative reconstruction while achieving high quality images with reduced data volumes, thus demonstrating the power of signal processing techniques for improving significantly the computational efficiency for solving nonlinear inverse problems. We note that randomized reconstruction for nonlinear imaging when the reconstruction step is optimized with regard to each random weights remains an open research problem. The theory of compressive sensing for linear

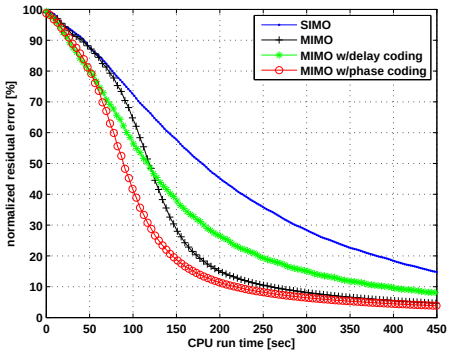

Figure 3.3: Convergence plots of iterative algorithms: SIMO vs. three MIMO waveform encoding schemes

inverse problems offers interesting insights and could lead to, combined with waveform encoding techniques, new fast and efficient EM full wave tomographic imaging algorithms for large scale imaging applications.

Bibliography

[Beal and Ghahramani, 2003] Beal, M. J. and Ghahramani, Z. (2003). The variational Bayesian EM algorithm for incomplete data: with application to scoring graphical model structures. In Bernardo, J. M. and Bayarri, M. J., editors, *Bayesian Statistics 7*, pages 453 – 463. University of Oxford Press.

[Braun et al., 2010] Braun, M., Sturm, C., and Jondral, F. K. (2010). Maximum likelihood speed and distance estimation for OFDM radar. In *Proceedings of IEEE Radar Conference*, pages 256 – 261. IEEE.

[Candes and Tao, 2006] Candes, E. J. and Tao, T. (2006). Near-optimal signal recovery from random projections: Universal encoding strategies? *IEEE Transactions on Information Theory*, 52(12):5406 – 5425.

[Candy, 2009] Candy, J. V. (2009). *Bayesian Signal Processing*. Wiley-IEEE Press, Hoboken, NJ.

[Chew, 1994] Chew, W. C. (1994). *Waves and Fields in Inhomogeneous Media*. IEEE Press, New York, NY.

[Chew and Wang, 1990] Chew, W. C. and Wang, Y. M. (1990). Reconstruction of two-dimensional permittivity distribution using the distorted born iterative method. *IEEE Transactions on Medical Imaging*, 9(4):218–225.

[Dong and Jin, 2013] Dong, C. and Jin, Y. (2013). MIMO nonlinear ultrasonic tomography by propagation and backpropagation method. *IEEE Transactions on Image Processing*, 22(3):1056–1069.

[Dong et al., 2012] Dong, C., Jin, Y., and Lu, E. (2012). Time domain electromagnetic tomography using propagation and backpropagation method. In *IEEE International Conference on Image Processing*, pages 2081–2084, Orlando, FL. IEEE.

[Dong et al., 2014] Dong, C., Jin, Y., and Lu, E. (2014). Accelerated nonlinear multichannel ultrasonic tomographic imaging using target sparseness. *IEEE Transactions on Image Processing*, 23(3):1379–1393.

[Dorn et al., 1999] Dorn, O., Bertete-Aguirre, H., Berryman, J. G., and Papanicolaou, G. C. (1999). A nonlinear inversion method for 3D electromagnetic imaging using adjoint fields. *Inverse Problems*, 15(6):1523–1558.

[Evans, 2010] Evans, L. C. (2010). *Partial Differential Equations*. American Mathematical Society, New York, NY, second edition.

[Fhager et al., 2006] Fhager, A., Hashemzadeh, P., and Persson, M. (2006). Reconstruction quality and spectral content of an electromagnetic time-domain inversion algorithm. *IEEE Transactions on Biomedical Engineering*, 53(8):1594–1604.

[Franchois and Pichot, 1997] Franchois, A. and Pichot, C. (1997). Microwave imaging complex permittivity reconstruction with a Levenberg-Marquardt method. *IEEE Transactions on Antennas and Propagation*, 45(2):203–214.

[Friston, 2010] Friston, K. (2010). The free-energy principle: a unified brain theory. *Nature Reviews Neuroscience*, 11:127–138.

[Garmatyuk et al., 2007] Garmatyuk, D., Schuerger, J., Morton, Y. T., Binns, K., Durbin, M., and Kimani, J. (2007). Feasibility study of a multi-carrier dual-use imaging radar and communication system. In *Radar Conference (EuRAD)*, pages 194–197.

[Gini et al., 2000] Gini, F., Greco, M. V., Diani, M., and Verrazzani, L. (2000). Performance analysis of two adaptive radar detectors against non-Gaussian real sea clutter data. *IEEE Transactions on Aerospace and Electronic Systems*, 36(4):1429–1439.

[Godwin and Sava,] Godwin, J. and Sava, P. CWP-645 Simultaneous source imaging by amplitude encoding. Colorado School of Mines.

[Greco et al., 2004] Greco, M., Bordoni, F., and Gini, F. (2004). X-band sea-clutter nonstationarity: Influence of long waves. *IEEE Journal of Oceanic Engineering*, 29(2):269–283.

[Han, 1977] Han, S.-P. (1977). A globally convergent method for nonlinear programming. *Journal of Optimization Theory and Applications*, 22(3):297309.

[Haykin, 2006] Haykin, S. (2006). Cognitive radar: a way of the future. *IEEE Signal Processing Magazine*, 23(1):30–40.

[Haykin et al., 2002] Haykin, S., Bakker, R., and Currie, B. W. (2002). Uncovering nonlinear dynamics - The case study of sea clutter. *Proceedings of the IEEE*, 90(5):860–881.

[He et al., 1997] He, S., Fuks, P., and Larson, G. W. (1997). An optimization approach to time-domain electromagnetic inverse problem for a stratified dispersive and dissipative slab. *IEEE Transactions on Antennas and Propagation*, 44(9):1277–1282.

[Isernia et al., 1997] Isernia, T., Pascazio, V., and Pierri, R. (1997). A nonlinear estimation method in tomographic imaging. *IEEE Transactions on Geoscience and Remote Sensing*, 35(4):910–923.

[Jia et al., 2002] Jia, H., Takenaka, T., and Tanaka, T. (2002). Time domain inverse scattering method for cross-borehold radar imaging. *IEEE Transactions on Geoscience and Remote Sensing*, 40(7):1640–1647.

[Jin et al., 2010] Jin, Y., Moura, J. M. F., and Donoughue, N. O. (2010). Time reversal in multiple-input multiple-output radar. *IEEE Journal of Selected Topics on Signal Processing*, 4(1):210–225.

[Kay, 1993] Kay, S. M. (1993). *Fundamentals of Statistical Signal Processing: Estimation Theory*. Prentice-Hall, Upper Saddle River, NJ.

[Krebs et al., 2009] Krebs, J. R., Anderson, J. E., Hinkley, D., Neelamani, R., Lee, S., Baumstein, A., and Lacasse, M.-D. (2009). Fast full-wavefield seismic inversion using encoded sources. *Geophysics*, 74(6):WCC177–WCC188.

[Lindley, 1980] Lindley, D. (1980). Approximate Bayesian methods. *Trabajos de Estadistica Y de Investigacion Operativa*, 31(1):223–245.

[Liu et al., 2002] Liu, Q. H., Zhang, Z. Q., Wang, T. T., Bryan, J. A., Bryan, G. A., Ybarra, G. A., Nolte, L. W., and Joines, W. T. (2002). Active microwave imaging I - 2-D forward and inverse scattering methods. *IEEE Transactions on Microwave Theory and Techniques*, 50(1):123–133.

[Lustig et al., 2008] Lustig, M., Donoho, D. L., Santos, J. M., and Pauly, J. M. (2008). Compressive sensing MRI. *IEEE Signal Processing Magzine*, 25(2):72 – 82.

[Mur, 1981] Mur, G. (1981). Absorbing boundary conditions for the finite-difference approximation of the time-domain electromagnetic-field equations. *IEEE Transactions on Electromagnetic Compatibility*, EMC-23(4):377–382.

[Ochiai and Imai, 2001] Ochiai, H. and Imai, H. (2001). On the distribution of the peak-to-average power ratio in OFDM signals. *IEEE Transactions on Communications*, 49(2):282–289.

[Paisley et al., 2012] Paisley, J., Blei, D., and Jordan, M. (2012). Variational Bayesian inference with stochastic search. In *Proceedings of the 29th International Conference on Machine Learning (ICML 2012)*, pages 1–8, Edinburgh, Scotland.

[Rife and Boorstyn, 1974] Rife, D. and Boorstyn, R. R. (1974). Single tone parameter estimation from discrete-time observations. *IEEE Transactions on Information Theory*, 20(5):591–598.

[Sangston and Gerlach, 1994] Sangston, K. J. and Gerlach, K. R. (1994). Coherent detection of radar targets in a non-Gaussian background. *IEEE Transactions on Aerospace and Electronic Systems*, 30(2):330–340.

[Schmidl and Cox, 1997] Schmidl, T. and Cox, D. (1997). Robust frequency and timing synchronization for OFDM. *IEEE Transactions on Communications*, 45(12):1613–1621.

[Sen and Nehorai, 2011] Sen, S. and Nehorai, A. (2011). Adaptive OFDM radar for target detection in multipath scenarios. *IEEE Transactions on Signal Processing*, 59(1):78–90.

[Sit et al., 2011] Sit, Y. L., Sturm, C., Reichardt, L., Zwick, T., and Wiesbeck, W. (2011). The OFDM joint radar-communication system: An overview. In *Proceedings of International Conference on Advances in Satellite and Space Communications*, pages 69–74.

[Smidl and Quinn, 2008] Smidl, V. and Quinn, A. (2008). Variational Bayesian filtering. *IEEE Transactions on Signal Processing*, 56(10):5020–5030.

[Testi et al., 2013] Testi, N., Xu, Y., and Jin, Y. (2013). Successive-MFCW modulation for ultra-fast narrowband radar. In *Proceedings of International Conference on Acoustics, Speech and Signal Processing (ICASSP)*, pages 6196–6200. IEEE.

[Turlapaty and Jin, 2013] Turlapaty, A. and Jin, Y. (2013). Parameter estimation and waveform design for cognitive radar by minimal free-energy principle. In *IEEE International Conference on Acoustics, Speech and Signal Processing*, pages 6244–6248.

[Tzikas et al., 2008] Tzikas, D. G., Likas, A. C., and Galatsanos, N. P. (2008). The variational approximation for Bayesian inference. *IEEE Signal Processing Magazine*, 25(6):131–146.

[Uchida et al., 1994] Uchida, M., Kagawa, Y., and Okuno, A. (1994). A vehicle-to-vehicle communication and ranging system based on spread spectrum techniques - SS communication radar. In *Proceedings of Vehicle Navagation and Information Systems Conference*, pages 169–174.

[Wang et al., 2006] Wang, J., Dogandzic, A., and Nehorai, A. (2006). Maximum likelihood estimation of compound-Gaussian clutter and target parameters. *IEEE Transactions on Signal Processing*, 54(10):3884–3898.

[Wright, 1968] Wright, J. W. (1968). A new model for sea clutter. *IEEE Transactions on Antennas and Propagation*, AP-16:217–223.